SubmilliJansky Transients in Archival Radio Observations

Geoffrey C. Bower, Destry Saul, Joshua S. Bloom[1], Alberto Bolatto, Alexei V. Filippenko,
Ryan J. Foley, and Daniel Perley

Department of Astronomy & Radio Astronomy Laboratory, University of California,
Berkeley, CA 94720-3411; gbower@astro.berkeley.edu

ABSTRACT

We report the results of a 944-epoch survey for transient sources with archival data from the Very Large Array spanning 22 years with a typical epoch separation of 7 days. Observations were obtained at 5 or 8.4 GHz for a single field of view with a full-width at half-maximum of $8.6'$ and $5.1'$, respectively, and achieved a typical point-source detection threshold at the beam center of $\lesssim 300$ μJy per epoch. The angular resolution ranged from $\sim 1''$ to $15''$. Ten transient sources were detected with a significance threshold such that only one false positive would be expected. Of these transients, eight were detected in only a single epoch. Two transients were too faint to be detected in individual epochs but were detected in two-month averages. None of the ten transients was detected in longer-term averages or associated with persistent emission in the deep image produced from the combination of all epochs. The cumulative rate for the short timescale radio transients above 370 μJy at 5 and 8.4 GHz is $0.07 \lesssim R \lesssim 40$ deg^{-2}yr^{-1}, where the uncertainty is due to the unknown duration of the transients, 20 min $\lesssim t_{char} \lesssim 7$ d. A two-epoch survey for transients will detect 1.5 ± 0.4 transient per square degrees above a flux density of 370 μJy. One transient is located ~ 3 kpc in projection from the nucleus of a spiral galaxy at a redshift $z = 0.040$. Based on the duration of the transient, its luminosity ($L \approx 2 \times 10^{38}$ erg s^{-1}), and its location in the galaxy, we suggest that it may be similar to the peculiar Type Ib/c radio supernova SN 1998bw associated with GRB 980428. The implied Type Ib/c rate is consistent to an order of magnitude with rates determined optically. A second transient is associated with a blue galaxy at $z = 0.249$ and may also be a luminous radio supernova or gamma-ray burst afterglow. Two other transient sources are possibly associated with the outer parts of faint, optically detected galaxies. The remaining six transients have no counterparts in the optical or infrared to limiting magnitudes of $R \approx 27$

---

[1]Sloan Research Fellow.

and $K_s \approx 18$ and show no faint persistent radio flux. For the eight transients without clear associations, known source classes of radio transients including radio supernovae, gamma-ray burst afterglows, active galactic nuclei, and stellar flares do not provide natural fits to the observed parameters. The hosts and progenitors of these transients are unknown.

Subject headings: radio continuum: general — radio continuum: stars — supernovae: general — gamma rays: bursts — surveys

1. Introduction

Radio transient sources have primarily been studied through follow-up observations after discovery at optical, X-ray, or γ-ray wavelengths (e.g., Hjellming et al. 1971; de Bruyn 1973; Frail et al. 1997; Eck et al. 2002; Frail et al. 1999; Gaensler et al. 2005), or through serendipitous discovery (e.g., Davies et al. 1976; Zhao et al. 1992; Bower et al. 2003). This is principally due to the high cost of observing time to survey large areas of sky to significant depth at radio wavelengths (Cordes et al. 2004). Moreover, existing blind surveys have typically been performed at low frequencies, where survey time is shorter but the effect of synchrotron self-absorption may hide certain source classes. The available parameter space for radio transient surveys is extensive: transients have been detected at, and are predicted for all, radio wavelengths; timescales of transient and variable behavior range from nanoseconds (Hankins et al. 2003) to the longest timescales probed (Hughes et al. 1992); and transients may originate from nearly all astrophysical environments including the solar system (Katz et al. 2003), star-forming regions (Bower et al. 2003), the Galactic Center (Zhao et al. 1992; Bower et al. 2005), and other galaxies (Frail et al. 1997).

Nevertheless, extensive surveys have been carried out, exploring different volumes of the parameter space, and, in some cases, discovering new phenomena. Roughly, one can separate transients surveys into two classes: (a) burst searches that probe timescales of less than ~ 1 second, are often performed with low angular resolution instruments, and are most often performed at low frequencies; and (b) imaging surveys conducted with interferometers which typically probe timescales of tens of seconds and longer. Examples of burst searches include STARE, a 611-MHz all-sky survey (Katz et al. 2003) sensitive to timescales of 0.1 s to a few minutes; a 843-MHz survey with the Molonglo Observatory synthesis Telescope (MOST) sensitive to timescales of 1 μs to 800 ms (Amy et al. 1989); and the Parkes 1.4-GHz multi-beam pulsar survey. STARE used dipole antennas with a sensitivity threshold of 27 kJy simultaneously over a significant fraction of the sky and found no extra-solar transients on timescales of 0.125 s to a few minutes in 18 months of observations. The

MOST survey determined an upper limit to the transient rate of 5 events s^{-1} deg^{-2} for 10 ms events at a flux density limit of 1 Jy. The Parkes multi-beam survey has been used for extensive searches for periodic emission as well as for pulsed emission. The latter search led to the discovery of rotating radio transients (RRATs), which appear to be pulsars with erratic emission (McLaughlin et al. 2006).

Imaging surveys for transients have focused on individual fields and on large-scale surveys. Recently, a blind survey of the Galactic center at 330 MHz has discovered an unusual radio transient that displays quasi-periodic emission on a timescale of 70 min (Hyman et al. 2005). Carilli et al. (2003) used $\sim$ 30 hr of observation of the Lockman hole to characterize variability on a timescale of 19 d and 17 mon at 1.4 GHz. They found no transients above 100 μJy and conclude that the transient density on these timescales is fewer than 18 per square degree. Similarly, Frail et al. (2003) identified 4 highly variable sources but no transient sources at 5 and 8.4 GHz using VLA observations of fields in which gamma-ray bursts are present. They set an upper limit to the variable source population of 6 deg^{-2} at sub-mJy sensitivity, comparable to the limit set by Carilli et al. (2003). Recently, drift scan interferometric observations have identified several transients of unknown origin, including a 3-Jy transient with a duration of 72 hr and three > 1 Jy transients of $i \lesssim 1$ d duration (Niinuma et al. 2007; Kuniyoshi et al. 2007; Matsumura et al. 2007).

The most extensive imaging search for transients derives from a comparison of the FIRST and NVSS 1.4 GHz catalogs (Levinson et al. 2002; Gal-Yam et al. 2006). The search covered 2400 square degrees at a flux density threshold of 6 mJy. This search generated a number of transient candidates. Of these, one source was identified as a radio supernova in a nearby galaxy and another was seen only once in the radio and could not be associated with any known optical source. Transient identification in this survey suffers from the methodological problem of the extremely mismatched resolutions (FIRST: 5$''$, NVSS: 45$''$) of the two surveys.

In addition to radio supernovae (RSNe), a number of highly variable and transient sources are expected to be detectable in significant numbers at radio wavelengths. One example is gamma-ray burst (GRB) afterglows associated with GRBs which are beamed in a direction away from Earth, and therefore not observable at high-energy wavelengths (Rhoads 1997). These so-called "orphan gamma-ray burst afterglows" (OGRBAs) are expected to outnumber GRBs by a factor of 10 to 1000, the specific value depending on the characteristics of the relativistic outflow of the GRB and the surrounding medium. There may be related phenomena such as those associated with X-ray flashes (Sakamoto et al. 2005), supernovae (SNe) (Berger et al. 2003), and short-duration GRBs (Gehrels et al. 2005). Activity from stars and compact objects in the Galaxy may also be detected as transients (e.g., Berger et al.

2001; Bower et al. 2005; Osten et al. 2006).

A range of active galactic nucleus (AGN) phenomena is also anticipated, including intra-day variability and other short-term variability driven by the effect of interstellar scintillation on compact components of extragalactic radio sources (e.g., Lovell et al. 2003). Intrinsic AGN variability is also expected. Sudden increases in the mass accretion rate following the tidal disruption of an orbiting star, for instance, will produce a transient soft X-ray flare and possibly radio emission (Rees 1988; Gezari et al. 2006).

Significant numbers of RSNe, OGRBAs, and tidal flares are predicted for surveys that achieve a sensitivity ~ 0.1 mJy and cover an area of ~ 10 square degrees. These phenomena all produce self-absorbed synchrotron radiation and, therefore, are more likely to be observed at high radio frequencies.

We describe here the results of a search for extragalactic radio transients using 5 and 8.4 GHz observations from the Very Large Array data archives. The survey includes 944 epochs over 22 years consisting of observations of the same field. At a sensitivity threshold of 370 μJy, the survey has an effective survey area comparable to that of a survey consisting of two epochs of 10 square degrees each, making this thus far the largest-area sub-mJy imaging survey of radio transient phenomena.

2. Observations and Analysis

2.1. The Archival Survey

Between 1983 and 2005, the VLA performed calibration and system check observations of the same blank field with a typical interval of ~ 7 d. Each epoch typically was 20 min in duration and consisted of 10 s integrations. The field is centered at $\alpha = 15^h 02^m 20.53^s$, $\delta = +78°16'14.905''$ (J2000). The field is out of the plane of the Galaxy ($l = 115°$, $b = 36°$). 626 epochs of observations were obtained at a frequency of 5 GHz between 1983 and 1999. 599 epochs were obtained at a frequency of 8.4 GHz between 1989 and 2005. VLA observations of this field ceased in 2005. Between 1989 and 1999, there was overlap between some of the 5 and 8.4 GHz observations. 281 of the 8.4 GHz epochs were simultaneously observed at 5 GHz, giving a total of 944 independent epochs at either frequency.

Data were all obtained in standard continuum mode with 50 MHz of bandwidth in each of two intermediate-frequency bands (with centers separated by 100 MHz) and two circular polarizations. We used a pipeline procedure for flagging, calibrating, and imaging. Phase calibration was made based on brief observations of the compact source J1803+784. Since no

standard flux density calibrator was used in these observations, we set the amplitude scale of the observations by assuming the mean flux density for J1803+784 as measured in the University of Michigan Radio Astronomy Observatory database over the same period (2.2 Jy and 2.8 Jy at 5 and 8.4 GHz, respectively Aller et al. 1999). The assumption of constant flux density introduces less than 15% uncertainty in the flux-density scale for individual epochs. Images of the target field typically had a root-mean-square (rms) error in the flux density of 40 to 50 μJy. Images from two successive epochs (19840613 and 19840620) are shown in Figure 1. Throughout the paper, we use the notation of YYYYMMDD to denote epoch date and refer to specific transients as RT YYYYMMDD, based on the epoch of detection.

Images were obtained in all configurations of the Very Large Array. For the extended configurations, bandwidth smearing within the primary beam can become significant. We compensated for this effect by applying a Gaussian taper with a full-width at half-maximum (FWHM) of 150 $k\lambda$ to the (u, v) data before imaging, which reduces sensitivity and angular resolution but provides imaging to large radii without bandwidth distortions. Images were made using natural weighting to achieve maximal sensitivity and were deconvolved using the CLEAN algorithm (Clark 1980). We imaged a region slightly larger than the region containing a circle of radius equal to twice the half-power radius, which is 9.0′ at 5 GHz and 5.4′ at 8.4 GHz.

A deep image of the region at 5 and 8.4 GHz was also constructed through merging of all visibilities and imaging with a (u, v) taper of 150 $k\lambda$ using the MIRIAD software package. The resulting images had resolutions of $\sim 5''$ and $\sim 3''$, and an rms of 2.6 μJy and 2.8 μJy at 5 and 8.4 GHz, respectively. The location of steady and transient radio sources on the deep image is shown in Figure 2. Fluxes in the deep image are typically lower than the average of detections since our high detection threshold and the low flux densities of the sources bias the mean. Further details of the deep images will be published separately.

2.1.1. Transient Identification

Sources were identified using AIPS task SAD (search and destroy), which identifies peaks in the image above a flux-density threshold and fits point sources. For the relatively uncluttered images that we have, SAD is efficient and accurate. We identified sources within twice the half-power radius and corrected their flux densities for primary beam losses.

The detection threshold for each image was chosen such that the probability of a false detection (PFD) in the full imaged region was 10^{-3}, or a single false source for 1000 identical epochs, assuming Gaussian statistics for noise in the image. Since the synthesized beam

changes with array configuration while the primary beam remains the same, the number of independent pixels in the field of view varied substantially. Detection thresholds were in the range $\sim 5\sigma$ to 6σ, dependent on array configuration. The typical flux density threshold at the center of the image was $\sim 300\ \mu$Jy. For the number of epochs observed and the circular area of the region searched for sources, we have an expectation of ~ 1 false source in the entire survey. Inverting the sign of the intensity in each image and searching for sources with the same thresholds and methods revealed one significant source, consistent with our expectations of one or fewer false detections in the entire survey.

Wider-field images ($\sim 40'$ at 5 GHz, $\sim 27'$ at 8.4 GHz) were made for all epochs in which a transient was detected. A number of transients that were detected on the western and northern edges of the individual epoch image were determined to be aliased power from two bright radio sources (~ 50 mJy) at radii greater than two primary beam widths (NVSS J1457+7817, J1500+7827). One source above the detection threshold was rejected on the basis of a non-pointlike image and deep negative stripes in the image.

Detected sources and their measured properties are listed in Tables 1 and 2. Table 1 identifies persistent sources above or near the detection threshold and not multiple-epoch transients. Six persistent sources at 5 GHz and 2 persistent sources at 8.4 GHz were detected in multiple epochs. The epochs of detection were distributed over the entire survey. Of these persistent sources, three radio sources with flux densities $> 500\ \mu$Jy were detected hundreds of times. One radio source (J150123+781806) was detected with our pipeline software at 5 GHz in 452 of 626 epochs, and at 8.4 GHz in 159 of 599 epochs (Figure 3); with a reduced source detection threshold of 3σ, we find that this source was present in 602 epochs at 5 GHz and in 445 epochs at 8.4 GHz. The results for this source indicate the overall quality of the data. Variations in the flux density of this source are caused by the changing sensitivity of the VLA in different configurations, variability in the amplitude calibrator J1803+784, and possibly intrinsic variability in the source.

Seven sources at 5 GHz and 1 source at 8.4 GHz were detected in individual epochs (Table 2). These sources were detected only once and are classified as transients. We plot the light curves of each transient for the year surrounding their detection (Figure 4).

We searched for time variability for each transient by splitting the data into four-minute segments and comparing the flux densities. The reduced χ^2 for the hypothesis of no variability is less than 1.4 for all the transients, implying no strong evidence for variability. We also imaged each transient in Stokes V and found no evidence for circular polarization above $\sim 30\%$. Finally, we differenced images between the intermediate frequency bands and found no evidence for a large spectral index.

The radial distribution of sources is consistent with a real source population rather than imaging defects. Imaging defects would be uniformly distributed throughout the image, without regard for the decline in sensitivity due to the primary beam. Four of the eight transients are contained within the half-power radius. This number is inconsistent with the expectation of a uniform distribution within the same region, 2.0 ± 1.4. On the other hand, a source population with a power-law distribution of flux densities $N(S) \propto S^{-3/2}$ in a flux-density limited sample has an expectation of 3.6 ± 1.3 within the half-power radius, in better agreement with the observed number.

Images were also constructed in a search for faint radiation from the transients and for new transients using all data from two-month, one-year, and one-decade time spans. We found two new transients in the two-month averages (Table 3) and no transients in the year and decade images. Light curves for these sources are shown in Figure 4. Given the smaller number of epochs, the expected number of false sources in the two-month average data is ~ 0.1. Further searches on different time scales or with filters matched to light curve shapes are possible with the same data but are beyond the scope of this paper.

Dual frequency observations were made only after 1989 and not at every epoch. Of the remaining 5 GHz transients, only 1 (RT 19920826) is located within the imaged region of the 8.4 GHz survey. Unfortunately, there were no 8.4 GHz observations for this epoch. Similarly, for RT 19970205 which was detected at 8.4 GHz, there was not a simultaneous 5 GHz observation.

2.2. Keck Imaging

On 25 July 2006 (UT dates are used throughout this paper), we observed the central portion of the radio field with the Low-Resolution Imaging Spectrometer (LRIS; Oke et al. 1995) on the Keck-I 10-m telescope. Eight of the radio transient positions (see Figure 6) were observed in two separate pointing centers (each covered by the LRIS field-of-view of $6' \times 7.8'$). At each pointing center we obtained six dithered 10-min exposures. The instrument is outfitted with a beam splitter, allowing us to observe simultaneously in the g and R bands. The data were reduced following standard optical imaging reduction procedures. After fitting a world coordinate system (tied to the USNO B1.0) to each reduced frame, we made a mosaic for a given filter using SWARP (Bertin et al. 2002). The final astrometric uncertainty relative to the International Celestial Reference System (ICRS) is 250 mas in each axis.

On the night of the Keck/LRIS imaging, we observed the Landolt standard star field

PG1633+099 (Landolt 1992) in both filters at an airmass of $\sec z = 1.04$. The catalog magnitudes were converted to the g band from the V-band magnitude and the $B - V$ color using the prescription in Bilir et al. (2005) . From the observed photometry of four PG1633+099 stars, the zeropoint conversion from flux in both filters was determined in an $0.6''$ aperture. The flux of 3σ-detected sources in both the R and g stacked image of the radio field were determined in the same-sized aperture. Accounting for the average extinction per unit airmass at Mauna Kea, we determine that the non-detections of some of the counterparts correspond to upper limits of $g(\mathrm{lim}) \approx 27.6$ and $R(\mathrm{lim}) \approx 26.55$ mag. These limits assume an unresolved source and a color similar to those of the Landolt field stars.

2.3.   Keck Spectroscopy

An optical spectrum of the counterpart of RT 19840613 was taken on 2005 Dec. 4 with the DEIMOS spectrograph (Faber et al. 2003) mounted on the Keck-II telescope, using a 600 line mm^{-1} grating and the GG400 order-blocking filter. Spectra of the counterparts and nearby companions of RTs 19860115, 19870422, 19920826, and 19970528 were taken on 2006 June 26 with LRIS using the 600/4000 grism, the 400/8500 grating, and the D560 dichroic.

All spectral data were reduced using standard techniques (e.g., Foley et al. 2003). Standard CCD processing and spectrum extraction were completed with IRAF[1]. The data were extracted with the optimal algorithm of Horne (1986). We obtained the wavelength scale from low-order polynomial fits to calibration-lamp spectra. Small wavelength shifts were applied after cross-correlating night-sky lines extracted with the object to a template sky. Using our own IDL routines, we fit spectrophotometric standard star spectra to flux calibrate our data and remove telluric lines (Wade & Horne 1988; Matheson et al. 2000).

We give redshifts for the counterparts and nearby companions in Table 4. In the cases of RTs 19840613, 19870422, 19920826, and 19970528, the redshift is for the galaxy that the RT is situated in or closest to. RT 19860115 has two possible hosts in the Keck image; Objects 1 and 2 are located to the northeast and southwest of the RT, respectively.

---

[1]IRAF is distributed by the National Optical Astronomy Observatory, which is operated by the Association of Universities for Research in Astronomy, Inc., under cooperative agreement with the National Science Foundation.

2.4. PAIRITEL Observations

Data were obtained with PAIRITEL (Bloom et al. 2006) on 16 Feb. 2006. Images were taken simultaneously in the J, H, and K_s bands in four different pointings with a total integration time of about 1120 s per pointing. Additionally, to get a deep infrared (IR) image in one portion of the radio field, several hours of imaging in June and July 2006 were obtained centered at J2000 position $\alpha = 15^h02^m36.0^s$, $\delta = +78°16'39''$. The approximate 3σ upper limits in the shallow, wide-angle map are $J = 19.2$ mag, $H = 18.5$ mag, and $K_s = 18.0$ mag (the limits are significantly worse toward the edges of the mosaic). The pointings were stitched together using SWARP after finding preliminary WCS solutions in all bands. The result is a 1050×1050 pixel set of mosaic images with $1'' \times 1''$ resolution that overlaps most of the radio image. An astrometric solution for the mosaic images was found through a cross-correlation with 43 stars in common with the USNO B1.0 catalog. Typical rms uncertainty of the astrometric tie to the ICRS is 250 mas.

3. Results

We have detected a total of 8 transient radio sources in single epochs of this survey (Figure 4). Additionally, we have detected two transients in two-month averages of the data. Our source identification methods described previously argue that no more than one of these sources is a false detection. All of these sources are adequately fit as point sources. None of the transients is detected in epochs other than the detection epoch, or in longer-term averages with the possible exception of RT 19840613, in which the host galaxy is detected in the full 20-year image.

In Figures 5 and 6 we show images of the transients overlaid on the deep radio image, on multi-color images from the Keck imaging, and, where Keck data are missing for two objects, on K_s-band images from PAIRITEL.

We identify several hosts or potential hosts to the RTs using the Minnesota Palomar Plate Survey (MAPS, http://aps.umn.edu; Pennington et al. 1993). MAPS is a catalog of sources found with and characterized by plate-measuring equipment surveying the Palomar Sky Survey I (POSS I). MAPS coordinates are consistent with the radio reference frame with an accuracy of $0.3''$. We confirmed this by comparison of the position of two bright reference stars in the MAPS catalog with positions in the Tycho catalog. Referring the Tycho positions to epoch 1950 (appropriate for POSS), we find agreement of $\sim 0.1''$ for GSC 04562-00668 and $\sim 1''$ for GSC 04562-00458.

3.1. A Transient Associated with a Spiral Galaxy: RT 19840613

One transient is of particular interest because it is coincident with a spiral galaxy at a redshift $z = 0.040$ (a distance of ~ 170 Mpc using $H_0 = 72 \mathrm{km}^{-1}\mathrm{Mpc}^{-1}$). The galaxy, identified as MAPS-P023-0189928, has $R = 16.5$ mag, $B - R = 1.8$ mag, and a major axis of $\sim 20''$. The transient is clearly non-nuclear; it is offset to the southwest of the optical nucleus by $2.7'' \pm 0.4''$, corresponding to a projected distance of 2.3 ± 0.3 kpc. The optical nucleus is coincident with the infrared nucleus as identified in the 2MASS catalog at an accuracy of $0.2''$. The probability of a single chance association with an optical source in the POSS at a few arcsecond precision is $\lesssim 1\%$. We calculate an isotropic radio luminosity of 2×10^{28} erg s^{-1} Hz^{-1}, or 2×10^{38} erg s^{-1} for a bandwidth of 10 GHz.

The transient is not detected in any other individual epoch, even with reduced detection thresholds. The transient is also not detected in any two-month average in the year surrounding its detection, nor is it detected in any annual average from the entire data set. It is also not detected in the year prior to detection, nor in the six years following detection. The absence of a detection in other light curves at 5 GHz is consistent with a rapid rise and a decline in the flux density with a power law of $t^{-\alpha}, \alpha > 0.5$.

The deep image of the region surrounding the transient shows extended radio continuum emission associated with the spiral galaxy and a companion galaxy (Figure 7). The location of the transient coincides with a region of peak emission, but it is not possible to conclude whether that emission is the result of the transient or a peak in the galactic emission. The peak of emission near the position of the transient is ~ 28 μJy, which corresponds to a star-formation rate of $< 0.1 M_\odot$ yr^{-1} (e.g., Yun & Carilli 2002).

The association of the transient with the non-nuclear region of a spiral galaxy, together with its luminosity, suggest that the transient may be a RSN. The transient is very unlikely to be a Type II RSN, as these sources exhibit rise and decay timescales of months to years, implying that a Type II RSN would be detected multiple times in our survey (Eck et al. 2002). Type Ia RSN have never been detected at radio wavelengths (Weiler et al. 2004). Type Ib/c RSN, on the other hand, evolve on timescales of days to months. The anomalous Type Ib/c RSN associated with SN 1998bw and GRB 980425 doubled its flux density during its rise and halved its flux density following the peak in < 10 d (Kulkarni et al. 1998). The light curve declined as t^{-1} with the exception of a brief period of increase attributed to clumpiness in the circumstellar medium. The luminosity of RT 19840613 places it among the brightest SNe Ib/c, although a factor of a few fainter than SN 1998bw (Berger et al. 2003). The luminosity of SN 2002ap, also a SN Ib/c, is four orders of magnitude less than that of SN 1998bw (Berger et al. 2003). The luminosity of RT 19840613 is three orders of magnitude less than the typical radio luminosity of a GRB afterglow.

3.2.   A Transient Associated with a Blue Galaxy: RT 19870422

RT 19870422 is located within $\sim 1.5''$ of the centroid of MAPS-P023-0189613. The Keck image shows that this RT is clearly associated with a blue galaxy and is significantly offset from the nucleus. The integrated R magnitude of the galaxy is 20.2, with $B - R = 2.5$ mag, and the redshift is determined to be $z = 0.249$ (or a distance of 1050 Mpc). Galaxy-template matching to the Keck spectrum shows it to most likely be an Sc galaxy with strong [O II] and [O III] emission, indicating current star formation.

The inferred isotropic radio luminosity is $L_\nu \approx 7 \times 10^{29}$ erg s^{-1} Hz^{-1}, or $L \approx 7 \times 10^{39}$ erg s^{-1} for a bandwidth of 10 GHz. RT 19870422 was detected in a two-month integration, implying a total energy release $E \approx 4 \times 10^{46}$ erg. We see no evidence for detection in other epochs, implying a source that fades with a timescale of two months or less following its peak. In the deep integration, we see that the galaxy is detected with an irregular morphology (Figure 8). The faint radio emission, however, is offset from the position of RT 19870422.

RT 19870422 shares many characteristics with RT 19840613. The RT position is clearly separated from the peak of the optical emission, ruling out the possibility of an AGN event. Its longer duration and higher luminosity, however, differentiate it. The luminosity is nearly an order of magnitude greater than that of SN 1998bw, and two orders of magnitude more luminous than the bright Type II SN 1979C (Eck et al. 2002). Thus, the luminosity falls in between the maximum observed luminosity of a RSN and the typical luminosity of a GRB afterglow. The two-month duration of RT 19870422 is more consistent with known RSNe of both Type Ib/c or Type II, as well as GRB afterglows.

3.3.   Transients Possibly Associated with Galaxies or Galaxy Groups: RT 19920826 & 19970528

RT 19920826 is located $\sim 5''$ to the southeast of a red galaxy identified in the Keck image, which is not identified in the MAPS catalog. The host is a red object with no clear emission or absorption lines.

RT 19970528 is located $\sim 5''$ to the northwest of MAPS-P023-0189499, which has $R = 19.6$ mag and $B - R = 2.4$ mag. Two other galaxies are identified within a radius of $30''$. The nearest one is a red, early-type galaxy at $z = 0.245$. Galaxy-template matching shows it is most likely an elliptical galaxy, but it is also well fit by an S0 spectrum.

We computed the probability of false association of these galaxies with transients through

Monte Carlo simulations. We randomly distributed 100,000 radio sources over the field and then measured the distance to the nearest galaxy as identified in the MAPS catalog. The probability of a false association at a distance of less than $5''$ is only 2%. The probability of a false association at a distance of $15''$ is $\sim 20\%$. The probability for any one of the 10 RTs being randomly associated with a galaxy at a distance of $5''$ is $\sim 20\%$, and at a distance of $15''$ the probability is nearly unity. The probability of multiple sources located within $5''$ is $\lesssim 5\%$. Thus, the association of either RT 19970528 or RT 19920826 or both RTs with a galaxy is probable but not certain.

3.4. Sources without Radio or Optical Counterparts: RT 19840502, 19860115, 19860122, 19970205, 19990504, & 20010331

There is no evidence for faint radio, optical, or infrared counterparts for six of our sources: RT 19840502, 19860115, 19860122, 19970205, 19990504, 20010331. There are no sources apparent in the image obtained by averaging the succeeding two months of data, as well as in the year-long and decade-long averages. These results require a rapidly decreasing light curve, proportional to t^{-1} or steeper.

RT 19860115 has two possible hosts. The first possible host, Object 1, is located $\sim 15''$ to the northeast of the RT and is a starburst galaxy at $z = 0.1297$ with strong emission lines and a blue continuum. Object 1 is identified as MAPS-P023-0190130, a galaxy with $R = 19.2$ mag and $B - R = 1.3$ mag, and is also detected as a faint, extended radio source. The other possible host, Object 2, is located $\sim 20''$ to the southwest of the RT and is an early-type galaxy at $z = 0.242$. Galaxy-template matching shows the spectrum is best fit by either an elliptical or S0 galaxy spectrum. Several other objects, likely to be galaxies, are in the field. The physical separation of RT 19860115 from the two objects is ~ 50–100 kpc, which is still within a radius at which the galaxy may contain stars. Nevertheless, given the Monte Carlo simulations discussed above, we conclude that this transient is likely associated only by chance with these galaxies.

For the remainder of sources, there are no obvious associations with galaxies or stars. The absence of optical or infrared counterparts only eliminates host candidates; the non-simultaneity of radio and optical observations implies that we place no limits on optical transients.

4. Radio Transient Rates

We can compute rates of transients in several different ways. We are limited in the accuracy of estimating transient rates by our lack of knowledge of the characteristic time scale, t_{char}, of the transient sources. This characteristic time falls between the duration of the observations (~ 20 min) and the typical separation between epochs (7 days).

The two-epoch survey sensitivity is independent of t_{char}. The effective area for a two-epoch survey for a given flux-density limit is just the sum of the areas in each epoch in which a source above the flux-density limit is detectable. For a set of N_e images with uniform sensitivity over a solid angle Ω in which N_t transients are detected, the two-epoch source density is $N_t(N_e - 1)^{-1}\Omega^{-1}$. For a sample with varying image properties, we can compute the two-epoch source density given the image noise statistics, the synthesized beam size, and the primary beam shape. The ratio of the primary beam solid angle to the synthesized beam solid angle gives the number of independent pixels in the image. The source detection threshold per image is then set based on the number of independent pixels and the rms noise. We combine the 5 GHz and 8.4 GHz survey limits and transient detections together. The accumulated results as a function of flux-density threshold are listed in Table 5.

We use a non-parametric Kaplan-Meier method (Feigelson & Nelson 1985), for estimating the cumulative source-count distribution and then compute transient rates (Figure 9). Seven transients are detected above a flux density of 370 μJy, giving a two-epoch source density of 1.5 ± 0.4 deg^{-2}. The transient rates are reasonably fit by a distribution with $S^{-\gamma}$ and $\gamma = 1.5$, which corresponds to a non-evolving, volume-limited sample. However, the constraints on γ are not very strong. A larger γ appears to be required to achieve agreement between the rate determined from this survey and the NVSS-FIRST survey (Gal-Yam et al. 2006). Different event rates at 1.4 and 5 GHz due to synchrotron self-absorption or other spectral index effects may also influence this comparison. Additionally, the FIRST-NVSS survey may be incomplete due to confusion from the mismatched resolution of these surveys.

We detected no transients in the 17 annual average images. The typical flux detection threshold at the half-power radius is 90 μJy. The total two-epoch area surveyed at this sensitivity is 0.3 deg^2, implying a 2σ upper limit to the two-epoch density for year-long transients at 90 μJy of ~ 6 deg^{-2}. In 96 images composed of two-month averages, we found two transients. At a flux-density threshold of 200 μJy, the effective area surveyed is 1.9 deg^2, giving a 2σ upper limit to the two-month transient rate of ~ 2 deg^{-2}.

We can also determine a rate as a function of area and time. The precision of this rate is limited by our lack of measurement of the characteristic time of the transient events. The rate for sources brighter than 370 μJy is then $0.07 < R < 40$ deg^{-2}yr^{-1}.

If we assume that RTs 19840613 and 19870422 belong to a distinct transient class based on their association with blue galaxies, we can estimate a rate for such transients as a function of volume and time. We could detect this transient to a distance of ~ 240 Mpc, which gives a total volume of ~ 300 Mpc^3. Assuming $t_{char} = 7$ d, we find a rate of 3×10^5 Gpc^{-3}yr^{-1}. Similarly for RT 19870422, we find a maximum volume of ~ 5000 Mpc^3 and use $t_{char} = 60$ d to find a rate of 4×10^3 Gpc^{-3}yr^{-1}. Jointly for RT 19840613 and RT 19870422, the rate is $\sim 2 \pm 2 \times 10^5$ Gpc^{-3}yr^{-1}. These rates are consistent within an order of magnitude of the SN Ib/c rate determined optically, 4.8×10^4 Gpc^{-3}yr^{-1} (Berger et al. 2003).

There is some evidence that our VLA field contains an overdensity of galaxies at $z \approx 0.25$ (Table 4). Additionally, the cluster Abell 2047 is located within $9'$ of the center of the VLA field (Abell et al. 1989). A2047 is a low-density cluster (richness class 0) with a radius $\sim 5'$ and a distance class of 6. The distance class is an estimate of distance based on visual inspection of photographic plates. The distance class of 6 is consistent with a redshift of 0.25 for the cluster (Struble & Rood 1987). If all the RTs are extragalactic, then the RT rates may be overestimated relative to the rate for the field by no more than a factor of a few.

5. Discussion

Two of the transients are reasonably identified as RSNe, possibly Type Ib/c or II and similar to known RSNe associated with GRBs. We consider now whether the eight transients not clearly identified with nearby galaxies are examples of known or expected classes of radio transients. These transients are unlikely to be RSNe unless they are associated with faint and/or low surface brightness galaxies. As we demonstrate below, the observed transient parameters do not easily fit into any expected class.

The known and anticipated sources of radio transients are very broad. Since we have no evidence for variability on a timescale of less than 20 min, we exclude from further discussion transient sources that have characteristic timescales of less than 1 s. These include pulsars and related phenomena such as RRATS and giant pulses (McLaughlin et al. 2006; Hankins et al. 2003; Cordes & McLaughlin 2003), as well as flares from extrasolar planets (Bastian et al. 2000; Lazio et al. 2004).

5.1.   X-ray Sources

Information on the X-ray properties of the transients and transient hosts is very limited. The ROSAT catalog of bright sources does not identify any sources in the field of our survey (Voges et al. 1999). There are also no sources in the RXTE All Sky Monitor catalog in the field, indicating an upper limit to the X-ray flux of events between 1997 and 2001 of ~ 10 mCrab (Swank 1999). No observations of the field have been made with the Chandra or XMM Newton X-ray Observatories.

5.2.   Gamma-Ray Burst Afterglows

Higher-energy counterparts to these transients have not been clearly detected. There are no known optically discovered SNe in the field of view of our survey, nor have there been any optical variability campaigns in this field. There are no GRBs which are uniquely localized to this field, although there are bursts with large positional uncertainties that could have originated in the field of view of our survey. We identify 7 BATSE events that occurred within 1σ of our field center between 1991 and 1999. Uncertainties in the BATSE positions, however, are $\sim 10°$, indicating a probability of $< 0.1\%$ for even one of these GRBs to have occurred within our field of view. Of the GRBs, one event (GRB 990508) occurred 4 d after RT 19990504. Given the low probability of concurrence and the lack (in other GRBs) of radio emission before gamma-ray emission, we conclude that this is almost certainly a coincidence. There is no systematic relationship between the remainder of the events and the radio transients.

5.3.   Orphan Gamma-Ray Burst Afterglows

In the standard paradigm of GRBs and GRB afterglows, the gamma-ray emission is highly anisotropic while the afterglow emission is less anisotropic or even isotropic. Thus, the observed GRBs and their afterglows from Earth are a subset of the total number of GRBs. Afterglows detected without gamma-ray emission are known as orphan gamma-ray burst afterglows. The ratio of OGRBAs to GRBs is the inverse of the beaming fraction, f_b^{-1} (e.g., Dalal et al. 2002). The phenomenon of a GRB afterglow without a corresponding gamma-ray burst has not been conclusively detected.

Detailed models of OGRBAs predict $\sim$1 per square degree at sensitivity thresholds of 0.1 mJy, which is consistent with our number of transient detections (Levinson et al. 2002; Totani & Panaitescu 2002). Whereas the canonical radio afterglow for the forward shock

rises on a timescale of days and decays slowly, the majority of the radio transients found in the present survey occur on timescales less than 1 week. One possible explanation in the context of GRB orphans is that the emission is due to the reverse shock, which is known, in the few cases where follow-up observations occurred soon after the GRB, to produce a bright and rapid (< 3 d) radio signature (Kulkarni et al. 1999; Frail 2003, e.g.,). Strong scintillation (Frail et al. 1997, e.g.,) of a standard, faint afterglow could also be responsible for producing short-term amplification that leads to an apparent fast transient, but then we might see marginal evidence for the forward shock in the epochs following the transient — yet this is not seen in individual sources.

The single long-timescale transient (RT 20010331) could be consistent with having arisen from the long-lived forward shock (as it transitions from mildly relativistic to nonrelativistic). Levinson et al. (2002) Levinson et al. (2002) calculate the expected number of forward-shock dominated OGRBAs for radio surveys. Taking the canonical interstellar medium density of $n_0 = 1$ cm^{-3}, it is reasonable to expect that we only find 1 viable forward-shock candidate with the nominal beaming of $f_b^{-1} = 500$. Nevertheless, since for the parameters of our survey we probe only to $z \approx 0.6$, the non-detection of an apparent host galaxy in deep Keck imaging of RT 20010331 would seem to suggest that our basic model assumptions for the radio afterglow are suspect.

Thus, the transients that we have detected can be considered consistent with the expectations of OGRBAs. There is, however, a large diversity of high-energy phenomena with poorly explored electromagnetic signatures beyond the classical GRB afterglow picture, including X-ray flashes, X-ray rich GRBs (Sakamoto et al. 2005), GRBs associated with SNe Ib/c (Berger et al. 2003), and short-duration GRBs (Gehrels et al. 2005). The richness of this phenomenology suggests that the radio transients we have discovered could reflect the continuum of stellar collapse events.

5.4. Active Galactic Nuclei

AGNs are highly variable and common. With the appropriate selection technique, AGNs can be found with a number density of > 100 per square degree (Stern et al. 2005). If our transients are AGNs, then the absence of deep, static detections indicates they are associated with radio-quiet objects, which constitute the majority of AGNs. Short-timescale variability of AGNs is often associated with interstellar scintillation and extreme scattering events, and typically has amplitudes of $\sim 10\%$ (Lovell et al. 2003). Variations of a factor of a few on timescales of hours have been seen in the most extreme cases such as PKS 0405-385 and J1819+3845, which is not sufficient to account for the observed transients given the very large

amplitude of variation observed (Rickett et al. 2002; Dennett-Thorpe & de Bruyn 2000).

Intrinsic variations among luminous AGNs are observed to have a timescale of months to years at radio frequencies (Hughes et al. 1992). Variations are rarely larger than a factor of a few in radio-loud objects. A survey of variable background sources in the direction of M31 found a small number of objects with variability of a factor of a few to 10 on timescales of years (Gelfand et al. 2005). An interesting example is the nucleus of the nearby spiral galaxy III Zw 2, which has exhibited factor of 20 fluctuations in its radio luminosity on timescales of months to years (Brunthaler et al. 2005). The TeV blazar Mrk 421 shows 50% variations on a timescale of ~ 10 d (Błażejowski et al. 2005). Sudden increases in the accretion rate, or shocks in the jet, could lead to a dramatic flare at radio wavelengths; however, these flares are expected to have timescales on the order of months to a year, inconsistent with our observations.

Recently discovered evidence for tidal disruption events in AGNs observed in the ultraviolet indicate the possibility for large-amplitude AGN transients (Gezari et al. 2006). However, the timescale for the observed UV transients are months to a year rather than days. Without a mechanism for a short timescale in the radio, tidal disruption events are unlikely to account for the observed radio transients.

5.5. Stellar Sources

We cannot exclude a Galactic origin for these transients. A wide range of stars and stellar systems are known to flare on timescales of minutes to hours to days. However, no known stellar types closely fit the properties of these transients. Our field ($b = 36°$, $l = 115°$) is out of the plane of the Galaxy, away from the Galactic center and bulge, and is not near any known star cluster or star-forming region. It is likely, therefore, that any stellar origin for these transients would be even more numerous in one of these more favored directions.

5.5.1. Known Luminous Transients

The luminosity of the observed transients is $L_\nu \approx 10^{18}(d/1 \text{ kpc})^2$ erg s^{-1} Hz^{-1}. This is near the upper limit of the known stellar radio luminosity distribution (Güdel 2002). RS CVn binaries, FK Com class stars, Algol-class stars, and T Tauri stars have been observed to radiate at this luminosity (e.g., Bower et al. 2003). The total number of known RS CVn, FK Com stars, and Algol stars discovered at X-ray wavelengths is < 1000, indicating that we are unlikely to detect any such objects by chance, even if the distance cutoff in our survey is

10 kpc (Dempsey et al. 1993). T Tauri stars are more common but are unlikely to be found outside regions of active star formation.

5.5.2. Late-Type Stars

M-type dwarfs at distances as large as 1 kpc have been identified as an important contribution to optical transient rates (Becker et al. 2004; Kulkarni & Rau 2006). Due to the typical low radio luminosity ($L_\nu \approx 10^{12} - 10^{14}$ erg s^{-1} Hz^{-1}) of known dMe stars and brown dwarfs, they are likely to be detected at distances of 30 pc or less. In an extreme case, the dMe star EV Lac was observed to undergo a flare of a factor of ~ 150 to a maximum luminosity $L_\nu \approx 10^{15}$ erg s^{-1} Hz^{-1}, with a rise time of minutes and a decay time of hours (Osten et al. 2006). Such a flare would be observed in our survey to a distance of 100 pc. The local space density of stars with $M < 0.3$ $M_\odot$ is 0.035 pc^{-3}, implying only a small chance of a low-mass star or brown dwarf within the volume to which we are sensitive (Reid et al. 1999). Any stellar origin for these transients must come from a faint source, since we have no detection of stellar counterparts in Keck, 2MASS, or PAIRITEL images. The 2MASS magnitude limit of $K_s = 15$ implies that any L dwarf ($M_K \approx 10$ mag) or earlier-type star must be at a distance > 100 pc to remain undetected. PAIRITEL limits require such stars to be at a distance > 500 pc. The limiting Keck magnitude requires late-type M stars to be at a distance > 1000 pc.

The probability distribution of radio activity in low-mass stars is not well quantified. Few stars have been observed at radio wavelengths for more than a few hours or a few days. Despite the lack of long-term monitoring of dMe stars, one can estimate the probability distribution of flares by comparison with the properties of the Sun. The probability of a solar flare at centimeter wavelengths of a given flux density S scales as $S^{-1.7}$ (Nita et al. 2004). ¿From observations of a large sample of late-type stars (Berger 2006), we estimate a probability of ~ 0.01 for a late-type star to exhibit a luminosity $L_\nu \approx 10^{15}$ erg s^{-1} Hz^{-1}. If the probability of stellar flares scales with the same relation as solar flares, a flare of $L_\nu \approx 10^{18}$ erg s^{-1} Hz^{-1} from a late-type star at a distance of 1 kpc would be visible in our radio survey but missing in the Keck image, and it would occur with a probability of $< 10^{-7}$. Assuming a constant density of stars set to the local value, the total number of M dwarfs out to 1 kpc within our field of view is $< 5 \times 10^3$. Given our ~ 1000 observations, the expected number of flares of this magnitude detected is $\lesssim 1$. This is an upper limit since the statistics for the observed stars are biased by selection for activity at other wavelengths. Within an order of magnitude, though, this matches the number of transients that we detect, suggesting that low-mass stars at 1 kpc or greater distance may contribute to, but are unlikely

to dominate, the observed radio-transient rate.

Very large radio flares might be accompanied by luminous X-ray flares. If the transients follow the radio/X-ray correlation (Güdel 2002), then a radio flare of 10^{18} erg s^{-1} Hz^{-1} at a distance of 1 kpc would have an X-ray luminosity of $10^{-9\pm1}$ erg s^{-1}, which exceeds the RXTE ASM detection threshold of $\sim 10^{-10}$ erg s^{-1}. However, many sources do not closely follow this relationship, including many low-mass stars (e.g., Berger et al. 2001).

5.5.3. Soft Gamma-Ray Repeaters

The transients share some properties with soft gamma-ray repeaters (SGRs). SGRs are magnetars that exhibit dramatic flares at gamma-ray and radio wavelengths (e.g., Frail et al. 1999; Gaensler et al. 2005). SGR 1806–20 produced a flare that reached a luminosity of 5×10^{22} erg s^{-1} Hz^{-1}, had a characteristic timescale of days, and declined as $t^{-2.7}$. Such a flare would be detectable in our dataset at a distance of ~ 200 kpc, would appear in only a single epoch, would fade away rapidly so that it is not seen in long-term averages, and would have no lasting optical counterpart. If all of our transients are Milky Way SGRs to a distance of $\lesssim 200$ kpc, the implied rate is $\gtrsim 0.01$ kpc^{-3} y^{-1} at high Galactic latitude. Without making any correction for Galactic population distribution, we estimate a total rate of $\gtrsim 3$ yr^{-1} in the disk of the Galaxy, which is at least an order of magnitude too high relative to the number of discovered SGRs.

5.5.4. X-ray Binaries

X-ray binaries (XRBs) can be seen throughout the Galaxy (e.g., Bower et al. 2005) but are rare (Muno et al. 2005). For the extremely overdense Galactic center, the XRB detection rate in the radio is $\lesssim 0.01$ kpc^{-3} yr^{-1}. The comparable observed transient rate would imply a similar overdensity at high Galactic latitude, which is implausible.

5.5.5. Pulsars

Most pulsar variability occurs on time scales much shorter than our observations and is therefore unlikely to account for our observed transients. There have been some examples, however, of longer timescale variability. PSR B1931+24, for instance, has periods of activity and inactivity with characteristic times of days to tens of days (Kramer et al. 2006). This variability is quasi-periodic, however, indicating that we would detect it and similar pulsars

in multiple epochs throughout our survey.

5.6.   Propagation Effects

We have already referred to the phenomenon of intra-day variability (IDV), which in the most extreme cases leads to variations of a factors of a few on a timescale of hours. IDV of this scale has been demonstrated to originate from interstellar scintillation of compact structure in the source. Galama et al. (1997) identified a factor of 43 fluctuation in the flux density of PSR B0655+64 at 325 MHz, which they argue originates from strong focusing in the interstellar medium — that is, a caustic. It is difficult to estimate the frequency with which such a phenomenon can occur, but observational evidence is scarce.

Microlensing could also produce a transient amplification of a background source. A simple calculation estimates that to explain all 10 RTs as the result of microlensing requires the product $n\tau \lesssim 10^{-2}$, where n is the number of sources that can be lensed and τ is the lensing opacity (Paczynski 1996). Since τ has been measured to be $\sim 10^{-7}$ by MACHO and OGLE experiments, then $n \gtrsim 10^9$, which is absurdly large for any known population of Galactic or extragalactic radio sources.

Finally, reflected solar flares off objects in the Solar System could produce detectable radio flares. A 1 MJy solar flare reflecting off a 1000 km object at a distance of 1 AU from the Earth would produce a 0.1 mJy flare at Earth. Our observed field is far out of the ecliptic plane, however, and there are few known Solar-System objects of this size outside of the ecliptic. Nearer objects could be smaller but would move significantly during the course of the observation.

6.   Conclusions

We have conducted a 944-epoch, 20-yr-long survey for radio transients with archival 5 and 8.4 GHz Very Large Array data. Ten radio transients are apparent in this data set. Eight transients appear in only a single epoch and disappear completely thereafter. Two transients appear in two-month integrations and also never reappear. We estimate the rate of radio transients below 1 mJy with a large uncertainty due to the wide range of characteristic times possible for these sources.

Two of the transients may be peculiar Type Ib/c and/or Type II radio SNe in nearby galaxies. All of these transients share some characteristics with those expected of orphan gamma-ray burst afterglows, but they cannot be conclusively identified as such. The diversity

of high-energy stellar-death phenomena makes it difficult to place specific limits on the nature of GRBs based on these results. The absence of persistent counterparts to these sources indicate that they are unlikely to be AGNs. Galactic sources appear unlikely to be an explanation, but they certainly cannot be ruled out. In particular, late-type stars could contribute to the number of radio transients if their luminosity distribution can be extrapolated by several orders of magnitude beyond the most luminous observed M-dwarf flare. Deeper multi-wavelength imaging is critical for identifying the hosts of these events.

In the near future, the Allen Telescope Array (DeBoer et al. 2004) will be efficient at discovering transients of this sort. The wide field of view of this telescope makes it a powerful instrument for large solid angle radio surveys. Given the apparently short timescale of these phenomena, rapid response to transient discovery at radio and other wavelengths will be critical for determining the nature of these transients.

REFERENCES

Abell, G. O., Corwin, H. G., & Olowin, R. P. 1989, ApJS, 70, 1

Aller, M. F., Aller, H. D., Hughes, P. A., & Latimer, G. E. 1999, ApJ, 512, 601

Amy, S. W., Large, M. I., & Vaughan, A. E. 1989, Proceedings of the Astronomical Society of Australia, 8, 172

Bastian, T. S., Dulk, G. A., & Leblanc, Y. 2000, ApJ, 545, 1058

Becker, A. C., Wittman, D. M., Boeshaar, P. C., Clocchiatti, A., Dell'Antonio, I. P., Frail, D. A., Halpern, J., Margoniner, V. E., Norman, D., Tyson, J. A., & Schommer, R. A. 2004, ApJ, 611, 418

Berger, E. 2006, ApJ, 648, 629

Berger, E., Ball, S., Becker, K. M., Clarke, M., Frail, D. A., Fukuda, T. A., Hoffman, I. M., Mellon, R., Momjian, E., Murphy, N. W., Teng, S. H., Woodruff, T., Zauderer, B. A., & Zavala, R. T. 2001, Nature, 410, 338

Berger, E., Kulkarni, S. R., Frail, D. A., & Soderberg, A. M. 2003, ApJ, 599, 408

Bertin, E., Mellier, Y., Radovich, M., Missonnier, G., Didelon, P., & Morin, B. 2002, in ASP Conf. Ser. 281: Astronomical Data Analysis Software and Systems XI, ed. D. A. Bohlender, D. Durand, & T. H. Handley, 228–+

Bilir, S., Karaali, S., & Tunçel, S. 2005, Astronomische Nachrichten, 326, 321

Błażejowski, M., Blaylock, G., Bond, I. H., Bradbury, S. M., Buckley, J. H., Carter-Lewis, D. A., Celik, O., Cogan, P., Cui, W., Daniel, M., Duke, C., Falcone, A., Fegan, D. J., Fegan, S. J., Finley, J. P., Fortson, L., Gammell, S., Gibbs, K., Gillanders, G. G., Grube, J., Gutierrez, K., Hall, J., Hanna, D., Holder, J., Horan, D., Humensky, B., Kenny, G., Kertzman, M., Kieda, D., Kildea, J., Knapp, J., Kosack, K., Krawczynski, H., Krennrich, F., Lang, M., LeBohec, S., Linton, E., Lloyd-Evans, J., Maier, G., Mendoza, D., Milovanovic, A., Moriarty, P., Nagai, T. N., Ong, R. A., Power-Mooney, B., Quinn, J., Quinn, M., Ragan, K., Reynolds, P. T., Rebillot, P., Rose, H. J., Schroedter, M., Sembroski, G. H., Swordy, S. P., Syson, A., Valcarel, L., Vassiliev, V. V., Wakely, S. P., Walker, G., Weekes, T. C., White, R., Zweerink, J., Mochejska, B., Smith, B., Aller, M., Aller, H., Teräsranta, H., Boltwood, P., Sadun, A., Stanek, K., Adams, E., Foster, J., Hartman, J., Lai, K., Böttcher, M., Reimer, A., & Jung, I. 2005, ApJ, 630, 130

Bloom, J. S., Starr, D. L., Blake, C. H., Skrutskie, M. F., & Falco, E. E. 2006, in ASP Conf. Ser. 351: Astronomical Data Analysis Software and Systems XV, ed. C. Gabriel, C. Arviset, D. Ponz, & S. Enrique, 751–+

Bower, G. C., Plambeck, R. L., Bolatto, A., McCrady, N., Graham, J. R., de Pater, I., Liu, M. C., & Baganoff, F. K. 2003, ApJ, 598, 1140

Bower, G. C., Roberts, D. A., Yusef-Zadeh, F., Backer, D. C., Cotton, W. D., Goss, W. M., Lang, C. C., & Lithwick, Y. 2005, ApJ, 633, 218

Brunthaler, A., Falcke, H., Bower, G. C., Aller, M. F., Aller, H. D., & Teräsranta, H. 2005, A&A, 435, 497

Carilli, C. L., Ivison, R. J., & Frail, D. A. 2003, ApJ, 590, 192

Clark, B. G. 1980, A&A, 89, 377

Cordes, J. M., Lazio, T. J. W., & McLaughlin, M. A. 2004, New Astronomy Review, 48, 1459

Cordes, J. M., & McLaughlin, M. A. 2003, ApJ, 596, 1142

Dalal, N., Griest, K., & Pruet, J. 2002, ApJ, 564, 209

Davies, R. D., Walsh, D., Browne, I. W. A., Edwards, M. R., & Noble, R. C. 1976, Nature, 261, 476

de Bruyn, A. G. 1973, A&A, 26, 105

DeBoer, D. R., Welch, W. J., Dreher, J., Tarter, J., Blitz, L., Davis, M., Fleming, M., Bock, D., Bower, G., Lugten, J., Girmay-Keleta, G., D'Addario, L. R., Harp, G. R., Ackermann, R., Weinreb, S., Engargiola, G., Thornton, D., & Wadefalk, N. 2004, in Ground-based Telescopes. Edited by Oschmann, Jacobus M., Jr. Proceedings of the SPIE, Volume 5489, pp. 1021-1028 (2004)., ed. J. M. Oschmann, Jr., 1021–1028

Dempsey, R. C., Linsky, J. L., Fleming, T. A., & Schmitt, J. H. M. M. 1993, ApJS, 86, 599

Dennett-Thorpe, J., & de Bruyn, A. G. 2000, ApJ, 529, L65

Eck, C. R., Cowan, J. J., & Branch, D. 2002, ApJ, 573, 306

Faber, S. M., Phillips, A. C., Kibrick, R. I., Alcott, B., Allen, S. L., Burrous, J., Cantrall, T., Clarke, D., Coil, A. L., Cowley, D. J., Davis, M., Deich, W. T. S., Dietsch, K., Gilmore, D. K., Harper, C. A., Hilyard, D. F., Lewis, J. P., McVeigh, M., Newman, J., Osborne, J., Schiavon, R., Stover, R. J., Tucker, D., Wallace, V., Wei, M., Wirth, G., & Wright, C. A. 2003, in Instrument Design and Performance for Optical/Infrared Ground-based Telescopes. Edited by Iye, Masanori; Moorwood, Alan F. M. Proceedings of the SPIE, Volume 4841, pp. 1657-1669 (2003)., ed. M. Iye & A. F. M. Moorwood, 1657–1669

Feigelson, E. D., & Nelson, P. I. 1985, ApJ, 293, 192

Foley, R. J., Papenkova, M. S., Swift, B. J., Filippenko, A. V., Li, W., Mazzali, P. A., Chornock, R., Leonard, D. C., & Van Dyk, S. D. 2003, PASP, 115, 1220

Frail, D. A. 2003, astro-ph/0309557

Frail, D. A., Kulkarni, S. R., Berger, E., & Wieringa, M. H. 2003, AJ, 125, 2299

Frail, D. A., Kulkarni, S. R., & Bloom, J. S. 1999, Nature, 398, 127

Frail, D. A., Kulkarni, S. R., Nicastro, S. R., Feroci, M., & Taylor, G. B. 1997, Nature, 389, 261

Gaensler, B. M., Kouveliotou, C., Gelfand, J. D., Taylor, G. B., Eichler, D., Wijers, R. A. M. J., Granot, J., Ramirez-Ruiz, E., Lyubarsky, Y. E., Hunstead, R. W., Campbell-Wilson, D., van der Horst, A. J., McLaughlin, M. A., Fender, R. P., Garrett, M. A., Newton-McGee, K. J., Palmer, D. M., Gehrels, N., & Woods, P. M. 2005, Nature, 434, 1104

Gal-Yam, A., Ofek, E. O., Poznanski, D., Levinson, A., Waxman, E., Frail, D. A., Soderberg, A. M., Nakar, E., Li, W., & Filippenko, A. V. 2006, ApJ, 639, 331

Galama, T. J., de Bruyn, A. G., van Paradijs, J., Hanlon, L., & Bennett, K. 1997, A&A, 325, 631

Gehrels, N., Sarazin, C. L., O'Brien, P. T., Zhang, B., Barbier, L., Barthelmy, S. D., Blustin, A., Burrows, D. N., Cannizzo, J., Cummings, J. R., Goad, M., Holland, S. T., Hurkett, C. P., Kennea, J. A., Levan, A., Markwardt, C. B., Mason, K. O., Meszaros, P., Page, M., Palmer, D. M., Rol, E., Sakamoto, T., Willingale, R., Angelini, L., Beardmore, A., Boyd, P. T., Breeveld, A., Campana, S., Chester, M. M., Chincarini, G., Cominsky, L. R., Cusumano, G., de Pasquale, M., Fenimore, E. E., Giommi, P., Gronwall, C., Grupe, D., Hill, J. E., Hinshaw, D., Hjorth, J., Hullinger, D., Hurley,

K. C., Klose, S., Kobayashi, S., Kouveliotou, C., Krimm, H. A., Mangano, V., Marshall, F. E., McGowan, K., Moretti, A., Mushotzky, R. F., Nakazawa, K., Norris, J. P., Nousek, J. A., Osborne, J. P., Page, K., Parsons, A. M., Patel, S., Perri, M., Poole, T., Romano, P., Roming, P. W. A., Rosen, S., Sato, G., Schady, P., Smale, A. P., Sollerman, J., Starling, R., Still, M., Suzuki, M., Tagliaferri, G., Takahashi, T., Tashiro, M., Tueller, J., Wells, A. A., White, N. E., & Wijers, R. A. M. J. 2005, Nature, 437, 851

Gelfand, J. D., Lazio, T. J. W., & Gaensler, B. M. 2005, ApJS, 159, 242

Gezari, S., Milliard, B., Martin, C., Halpern, J. P., & Basa, S. 2006, in IAU Symposium

Güdel, M. 2002, ARA&A, 40, 217

Hankins, T. H., Kern, J. S., Weatherall, J. C., & Eilek, J. A. 2003, Nature, 422, 141

Hjellming, R. M., Wade, C. M., Hughes, V. A., & Woodsworth, A. 1971, Nature, 234, 138

Horne, K. 1986, PASP, 98, 609

Hughes, P. A., Aller, H. D., & Aller, M. F. 1992, ApJ, 396, 469

Hyman, S. D., Lazio, T. J. W., Kassim, N. E., Ray, P. S., Markwardt, C. B., & Yusef-Zadeh, F. 2005, Nature, 434, 50

Katz, C. A., Hewitt, J. N., Corey, B. E., & Moore, C. B. 2003, PASP, 115, 675

Kramer, M., Lyne, A. G., O'Brien, J. T., Jordan, C. A., & Lorimer, D. R. 2006, Science, 312, 549

Kulkarni, S. R., Frail, D. A., Sari, R., Moriarty-Schieven, G. H., Shepherd, D. S., Udomprasert, P., Readhead, A. C. S., Bloom, J. S., Feroci, M., & Costa, E. 1999, ApJ, 522, L97

Kulkarni, S. R., Frail, D. A., Wieringa, M. H., Ekers, R. D., Sadler, E. M., Wark, R. M., Higdon, J. L., Phinney, E. S., & Bloom, J. S. 1998, Nature, 395, 663

Kulkarni, S. R., & Rau, A. 2006, ApJ, 644, L63

Kuniyoshi, M., Matsumura, N., Takefuji, K., Niinuma, K., Kida, S., Takeuchi, A., Nakamura, R., Suzuki, S., Tanaka, T., Asuma, K., & Daishido, T. 2007, PASP, 119, 122

Landolt, A. U. 1992, AJ, 104, 340

Lazio, T., Joseph, W., Farrell, W. M., Dietrick, J., Greenlees, E., Hogan, E., Jones, C., & Hennig, L. A. 2004, ApJ, 612, 511

Levinson, A., Ofek, E. O., Waxman, E., & Gal-Yam, A. 2002, ApJ, 576, 923

Lovell, J. E. J., Jauncey, D. L., Bignall, H. E., Kedziora-Chudczer, L., Macquart, J.-P., Rickett, B. J., & Tzioumis, A. K. 2003, AJ, 126, 1699

Matheson, T., Filippenko, A. V., Ho, L. C., Barth, A. J., & Leonard, D. C. 2000, AJ, 120, 1499

Matsumura, N., Daishido, T., Kuniyoshi, M., Asuma, K., Takefuji, K., Niinuma, K., Kida, S., Takeuchi, A., Nakamura, R., Shigehiro, S., & Tanaka, T. 2007, AJ, 133, 1441

McLaughlin, M., Lyne, A., Lorimer, D., Kramer, M., Faulkner, A., Manchester, R., Cordes, J., Camilo, F., Possenti, A., Stairs, I., Hobbs, G., D'Amico, N., Burgay, M., & O'Brien, J. 2006, Nature, 439, 817

Muno, M. P., Pfahl, E., Baganoff, F. K., Brandt, W. N., Ghez, A., Lu, J., & Morris, M. R. 2005, ApJ, 622, L113

Niinuma, K., Asuma, K., Kuniyoshi, M., Matsumura, N., Takefuji, K., Kida, S., Takeuchi, A., Nakamura, R., Tanaka, T., Suzuki, S., & Daishido, T. 2007, ApJ, 657, L37

Nita, G. M., Gary, D. E., & Lee, J. 2004, ApJ, 605, 528

Oke, J. B., Cohen, J. G., Carr, M., Cromer, J., Dingizian, A., Harris, F. H., Labrecque, S., Lucinio, R., Schaal, W., Epps, H., & Miller, J. 1995, PASP, 107, 375

Osten, R. A., Hawley, S. L., Allred, J., Johns-Krull, C. M., Brown, A., & Harper, G. M. 2006, ApJ, 647, 1349

Paczynski, B. 1996, ARA&A, 34, 419

Pennington, R. L., Humphreys, R. M., Odewahn, S. C., Zumach, W., & Thurmes, P. M. 1993, PASP, 105, 521

Rees, M. J. 1988, Nature, 333, 523

Reid, I. N., Kirkpatrick, J. D., Liebert, J., Burrows, A., Gizis, J. E., Burgasser, A., Dahn, C. C., Monet, D., Cutri, R., Beichman, C. A., & Skrutskie, M. 1999, ApJ, 521, 613

Rhoads, J. E. 1997, ApJ, 487, L1+

Rickett, B. J., Kedziora-Chudczer, L., & Jauncey, D. L. 2002, ApJ, 581, 103

Sakamoto, T., Lamb, D. Q., Kawai, N., Yoshida, A., Graziani, C., Fenimore, E. E., Donaghy, T. Q., Matsuoka, M., Suzuki, M., Ricker, G., Atteia, J.-L., Shirasaki, Y., Tamagawa, T., Torii, K., Galassi, M., Doty, J., Vanderspek, R., Crew, G. B., Villasenor, J., Butler, N., Prigozhin, G., Jernigan, J. G., Barraud, C., Boer, M., Dezalay, J.-P., Olive, J.-F., Hurley, K., Levine, A., Monnelly, G., Martel, F., Morgan, E., Woosley, S. E., Cline, T., Braga, J., Manchanda, R., Pizzichini, G., Takagishi, K., & Yamauchi, M. 2005, ApJ, 629, 311

Stern, D., Eisenhardt, P., Gorjian, V., Kochanek, C. S., Caldwell, N., Eisenstein, D., Brodwin, M., Brown, M. J. I., Cool, R., Dey, A., Green, P., Jannuzi, B. T., Murray, S. S., Pahre, M. A., & Willner, S. P. 2005, ApJ, 631, 163

Struble, M. F., & Rood, H. J. 1987, AJ, 93, 1035

Swank, J. H. 1999, Nuclear Physics B Proceedings Supplements, 69, 12

Totani, T., & Panaitescu, A. 2002, ApJ, 576, 120

Voges, W., Aschenbach, B., Boller, T., Bräuninger, H., Briel, U., Burkert, W., Dennerl, K., Englhauser, J., Gruber, R., Haberl, F., Hartner, G., Hasinger, G., Kürster, M., Pfeffermann, E., Pietsch, W., Predehl, P., Rosso, C., Schmitt, J. H. M. M., Trümper, J., & Zimmermann, H. U. 1999, A&A, 349, 389

Wade, R. A., & Horne, K. 1988, ApJ, 324, 411

Weiler, K. W., van Dyk, S. D., Sramek, R. A., & Panagia, N. 2004, New Astronomy Review, 48, 1377

Yun, M. S., & Carilli, C. L. 2002, ApJ, 568, 88

Zhao, J., Roberts, D. A., Goss, W. M., Frail, D. A., Lo, K. Y., Subrahmanyan, R., Kesteven, M. J., Ekers, R. D., Allen, D. A., & Burton, M. G. 1992, Science, 255, 1538

Table 1.   Steady Sources Detected in at Least One Epoch

RA (J2000)	Dec. (J2000)	N_{det}	$<S>$ (μJy)	S_{deep} (μJy)
	5 GHz			
15 00 11.48 ± 0.10	78 12 42.26 ± 00.13	26	2380 ± 73	502 ± 17
15 00 44.87 ± 0.10	78 18 39.04 ± 00.32	4	874 ± 36	180 ± 7
15 01 11.70 ± 0.10	78 15 20.23 ± 00.10	141	504 ± 6	307 ± 4
15 01 16.19 ± 0.10	78 12 45.88 ± 00.10	363	1146 ± 14	741 ± 5
15 01 22.67 ± 0.10	78 18 05.66 ± 00.10	452	880 ± 9	634 ± 3
15 02 51.40 ± 0.10	78 18 12.46 ± 00.10	23	351 ± 19	155 ± 3
15 03 24.83 ± 0.14	78 17 37.62 ± 00.46	1	318 ± 54	166 ± 4
15 03 28.07 ± 0.30	78 09 21.50 ± 01.04	1	2045 ± 301	2650 ± 8
	8.4 GHz			
15 01 11.13 ± 0.12	78 15 22.45 ± 00.32	1	1081 ± 154	291 ± 9
15 01 22.58 ± 0.10	78 18 05.80 ± 00.10	159	1099 ± 36	794 ± 8
15 02 51.38 ± 0.10	78 18 13.14 ± 00.18	3	518 ± 31	225 ± 4
15 03 23.41 ± 0.41	78 17 35.74 ± 00.64	1	840 ± 157	212 ± 8

Note. — Columns are (1) right ascension, (2) declination, (3) the number of epochs in which the source is detected, (4) mean flux density of detections, and (5) flux density in the deep image.

Table 2.   Transient Sources from a Single Epoch

Epoch	RA (J2000)	Dec. (J2000)	S (μJy)	S_{deep} (μJy)	t_{next} (days)	S_{next} (μJy)	$-\log_{10} PFD$	Host
		5 GHz						
19840502	15 02 24.61 ± 0.21	78 16 10.08 ± 00.46	448 ± 74	< 8	7	−10 ± 68	4.5	X
19840613	15 01 38.07 ± 0.21	78 18 40.75 ± 00.39	566 ± 81	< 28	7	86 ± 89	7.5	G
19860115	15 02 26.40 ± 0.44	78 17 32.39 ± 01.59	370 ± 67	< 8	7	199 ± 121	3.6	X
19860122	15 00 50.15 ± 0.34	78 15 39.37 ± 01.38	1586 ± 248	< 15	7	−59 ± 164	6.4	X
19920826	15 02 59.89 ± 0.35	78 16 10.82 ± 02.44	642 ± 101	< 9	56	37 ± 83	6.3	?
19970528	15 00 23.55 ± 0.10	78 13 01.37 ± 00.17	1731 ± 232	< 36	7	90 ± 206	7.9	?
19990504	14 59 46.42 ± 0.56	78 20 29.03 ± 00.74	7042 ± 963	< 117	21	−313 ± 1020	9.1	X
		8.4 GHz						
19970205	15 01 29.35 ± 0.10	78 19 49.20 ± 00.10	2234 ± 288	< 646	5	857 ± 323	8.0	X

Note. — Columns are (1) RT epoch, (2) right ascension, (3) declination, (4) mean flux density of detection, (5) flux density in the deep image, (6) separation in days between next epoch and epoch of transient, (7) flux density in the next epoch, (8) the negative logarithm of the probability of false detection in the single epoch, and (9) optical/IR host identification, where "G" indicates galaxy, "?" indicates possible galaxy association, and "X" indicates no host.

Table 3.   Transient Sources with $T_{\mathrm{char}} = 2$ months

Epoch	RA (J2000)	Dec. (J2000)	S (μJy)	S_{deep} (μJy)	t_{next} (days)	S_{next} (μJy)	$-\log_{10} PFD$	Host
			5 GHz					
19870422	15 00 50.01 $\pm$ 0.35	78 09 45.49 $\pm$ 0.97	505 ± 83	< 36	96	-154 ± 65	3.0	G
			8.4 GHz					
20010331	15 03 46.18 $\pm$ 0.10	78 15 41.68 $\pm$ 00.11	697 ± 94	< 37	59	85 ± 85	3.4	X

Note. — Columns are (1) RT epoch, (2) right ascension, (3) declination, (4) mean flux density of detection, (5) flux density in the deep image, (6) separation in days between next epoch and epoch of transient, (7) flux density in the next epoch, (8) the negative logarithm of the probability of false detection in the single epoch, and (9) optical/IR host identification, where "G" indicates galaxy, "?" indicates possible galaxy association, and "X" indicates no host.

Table 4.   Magnitudes, Colors, and Redshifts of Transient Host Galaxies

RT Epoch	MAPS Counterpart	Host Offset	R (mag)	$B - R$ (mag)	z
19840613	P023-0189928	2.7″ NW	16.5	1.8	0.040
19860115-1	P023-0190130	15″ NE	19.2	1.3	0.130
19860115-2	. . .	20″ SW			0.242
19870422	P023-0189613	1.5″ SE	20.2	2.5	0.249
19920826	. . .	5″ NW			unknown
19970528	P023-0189499	5″ SE	19.6	2.4	0.245

Note. — Host offset is position relative to the transient. Magnitudes and colors are from MAPS catalog.

Table 5.   Effective Area Searched for a Comparable Two-Epoch Survey

Flux Density (μJy)	5 GHz Number of Epochs	Area (deg^2)	8.4 GHz Number of Epochs	Area (deg^2)	Total Number of Epochs	Area (deg^2)
70	9	0.16	0	0.0	9	0.16
100	10	0.24	0	0.0	10	0.24
140	12	0.34	0	0.0	12	0.34
200	35	0.50	0	0.0	35	0.50
280	201	1.42	442	1.45	435	2.19
400	464	4.57	560	3.08	761	6.20
560	561	9.14	584	4.79	873	11.68
800	596	14.56	591	6.64	910	18.09
1120	606	19.85	591	8.40	924	24.31
1600	607	25.51	598	10.28	925	30.97

Table 6.   Effective Area Searched for a Comparable Two-Epoch Survey for $T_{\rm char} = 2$ months

Flux Density (μJy)	5 GHz Number of Epochs	Area (deg^2)	8.4 GHz Number of Epochs	Area (deg^2)	Total Number of Epochs	Area (deg^2)
70	24	0.10	9	0.02	26	0.1
100	41	0.49	38	0.22	54	0.56
140	55	0.91	61	0.67	73	1.11
200	75	1.51	74	1.31	99	1.91
280	90	2.24	78	1.97	115	2.84
400	95	3.11	78	2.69	120	3.94
560	95	3.93	78	3.37	120	4.97
800	95	4.81	78	4.09	120	6.07
1120	95	5.64	78	4.77	120	7.11
1600	95	6.52	78	5.48	120	8.22
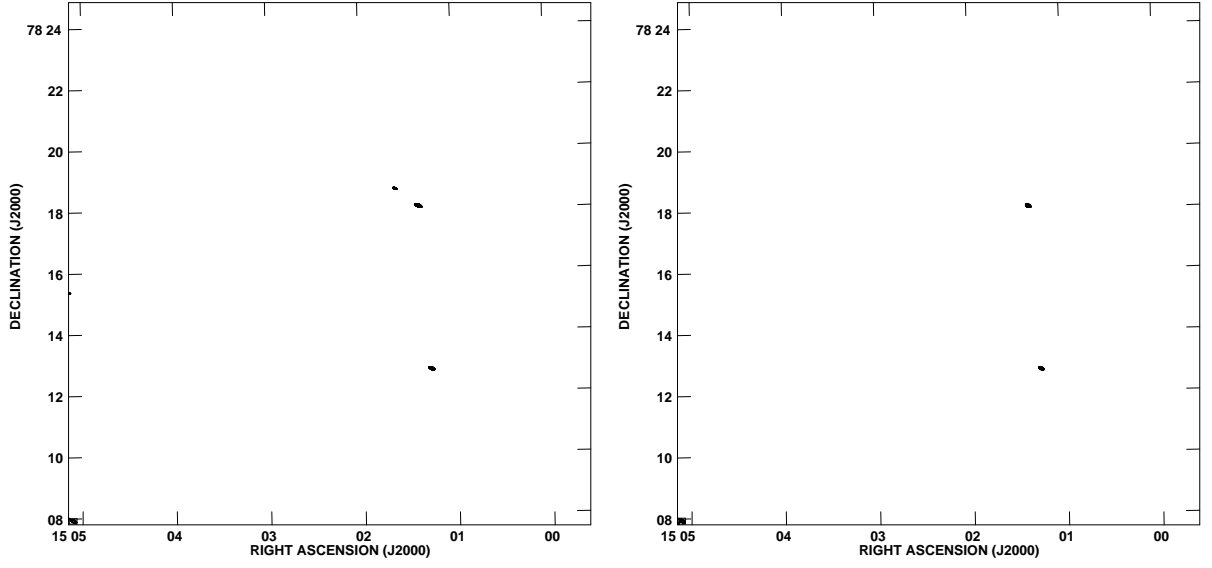
Fig. 1.— Image from epochs 19840613 (left) and 19840620 (right) at 5 GHz. The two westernmost sources are steady sources J150112+781520 and J150123+781806. The northernmost source is a transient, J150138+781841, detectable only in epoch 19840613. Contours are 5, 6, and 7 times the image rms of 57 and 63 μJy.
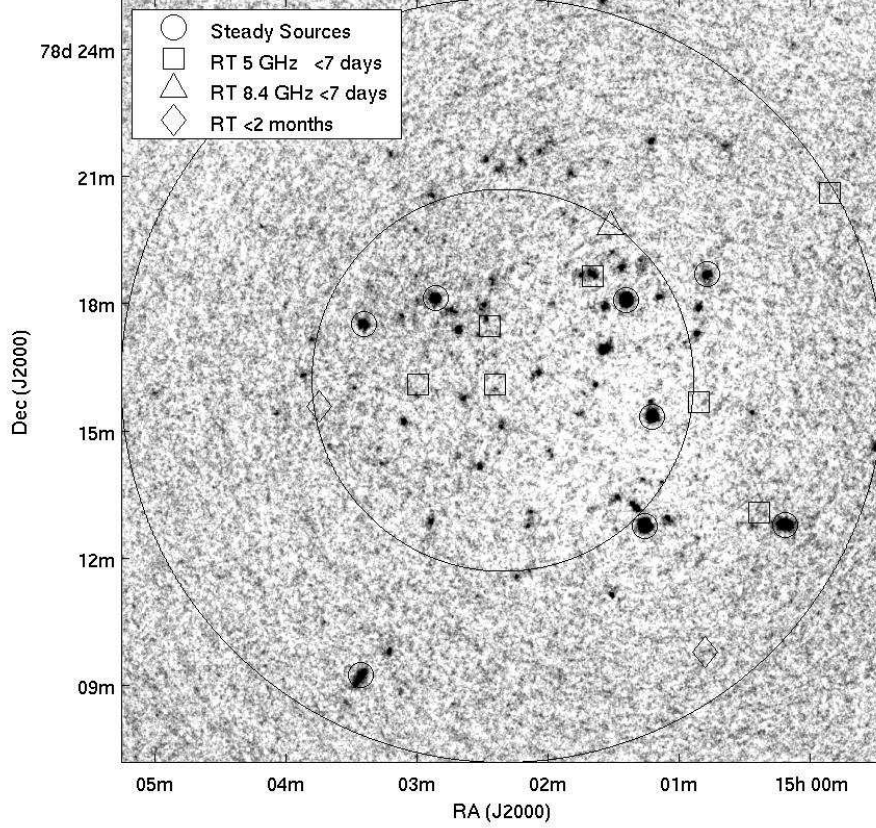
Fig. 2.— Deep image obtained at 5 GHz. We show the positions of single-epoch transient sources at 5 GHz (squares), single-epoch transient source at 8.4 GHz (triangle), two-month epoch transient sources (diamonds), and steady sources detected at least once in an individual epoch (circles). The two large circles indicate the half-power radius and twice the half-power radius of the 5-GHz field. The grey scale stretches from -2.5 to 30 μJy. The image has not been corrected for primary beam attenuation.
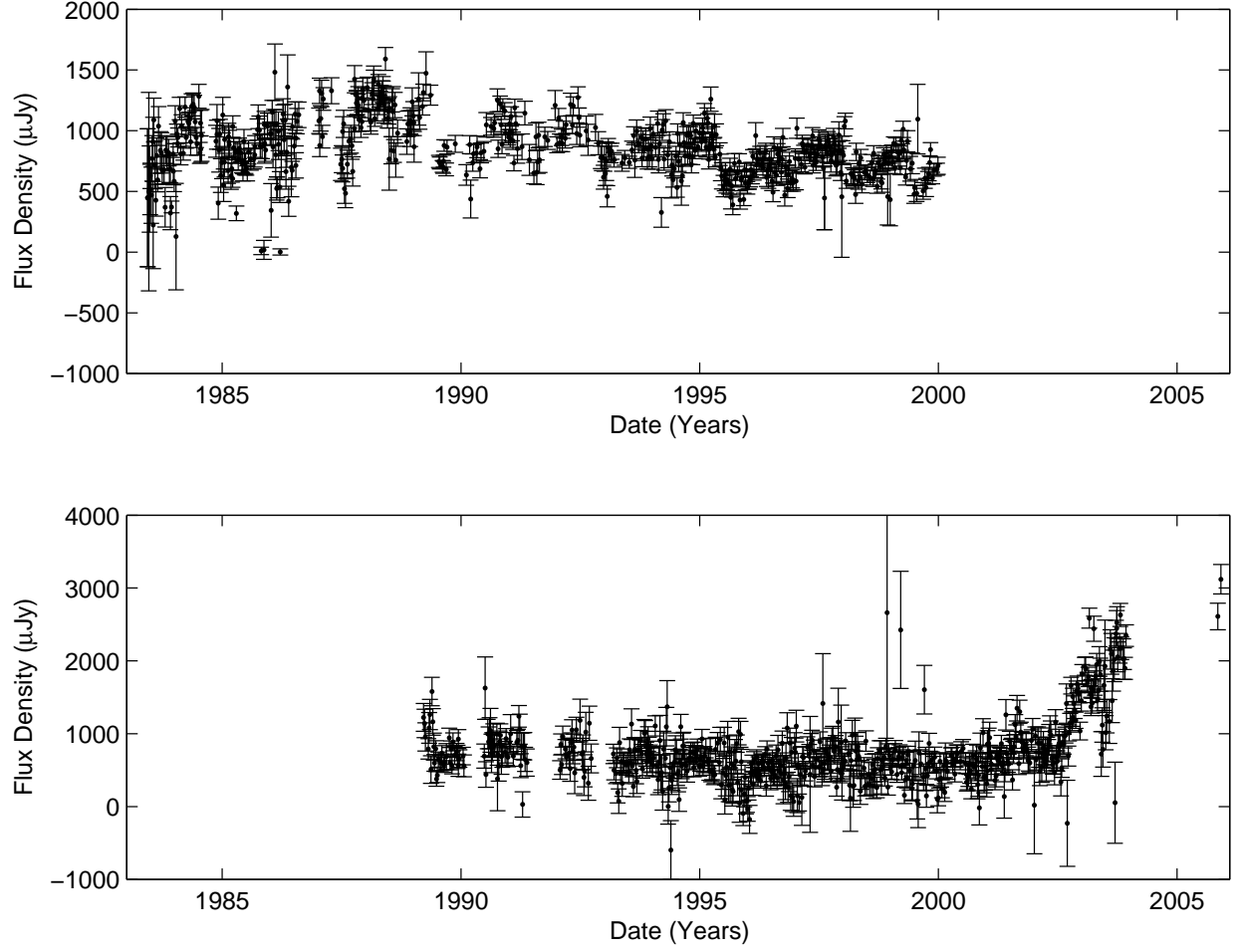
Fig. 3.— Light curve of J150123+781806 at 5 GHz (top) and 8.4 GHz (bottom) from the entire data set.
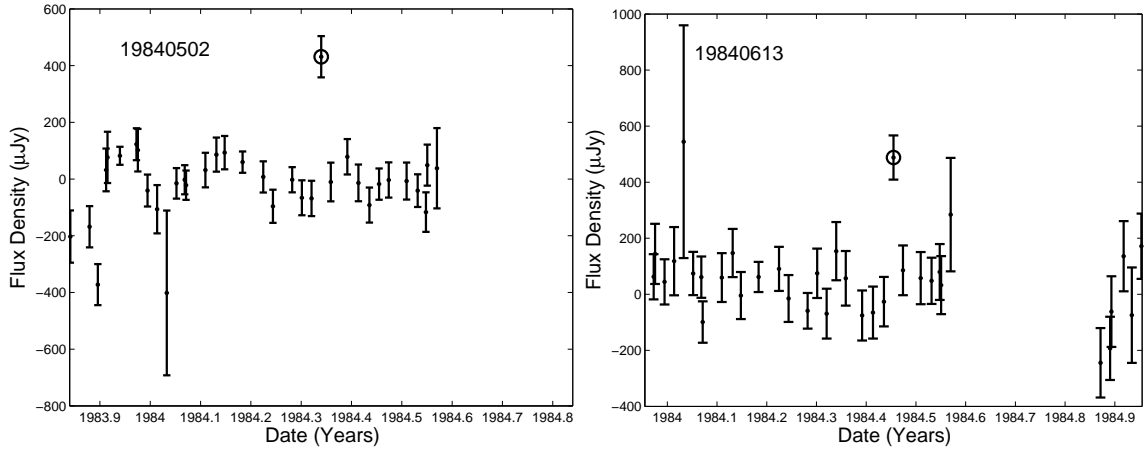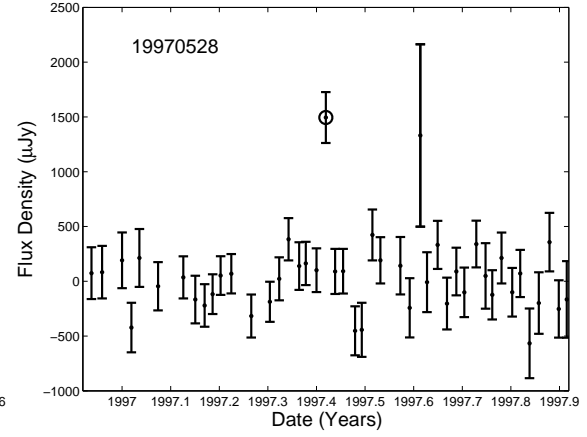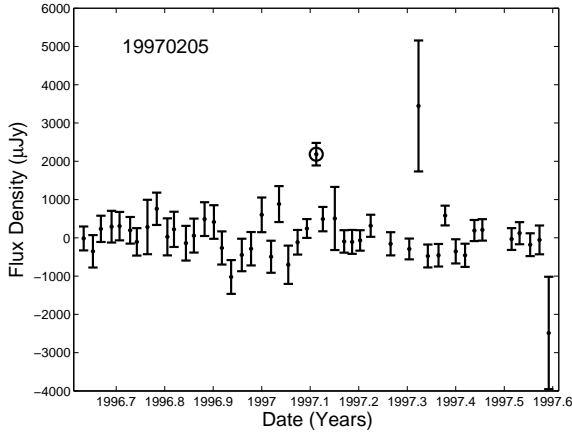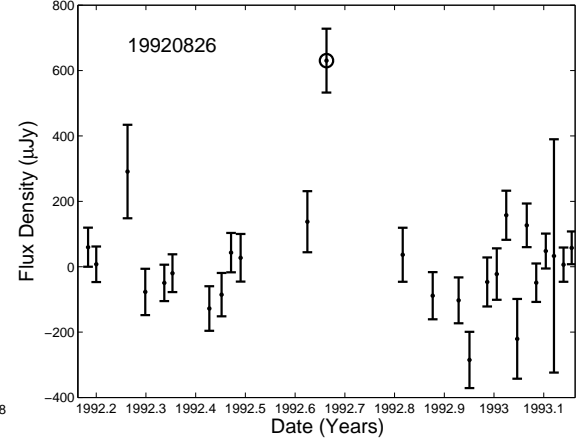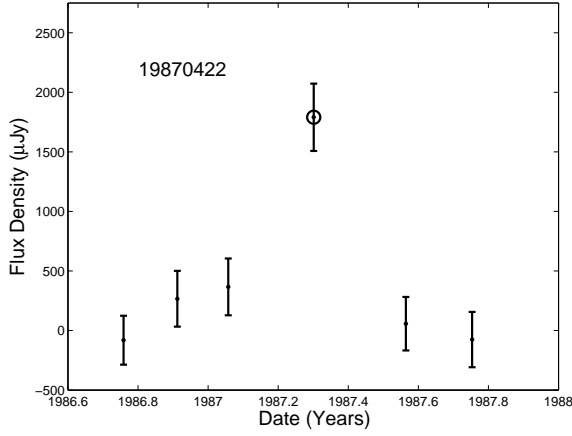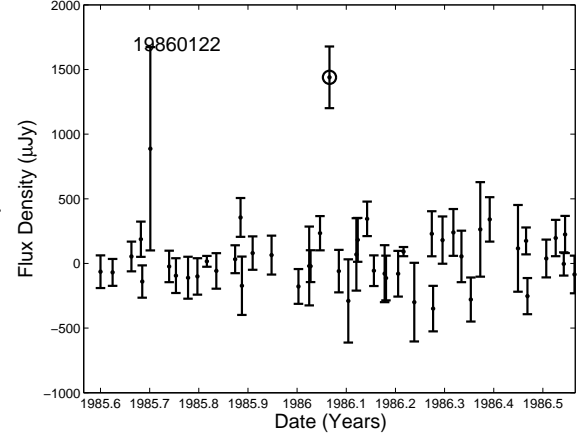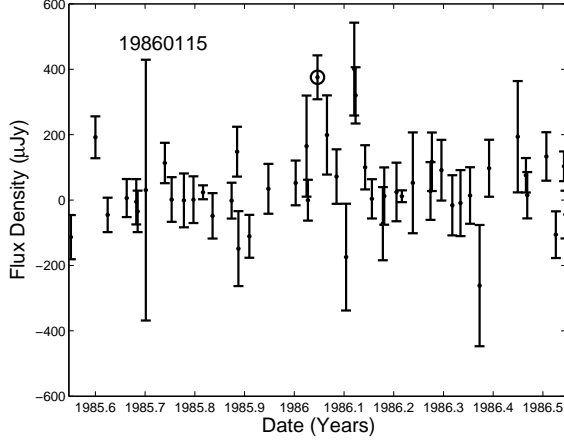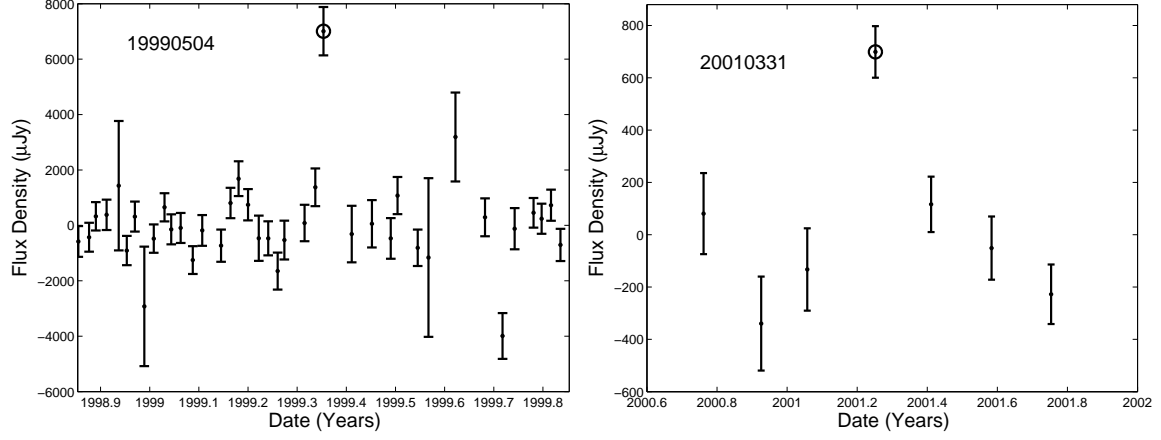
Fig. 4.— Light curves of the transient sources for the year surrounding detection. A circle around the point denotes the epoch of detection. Other points for all sources are all non-detections; values given are best-fit Gaussians at the position of the transient.
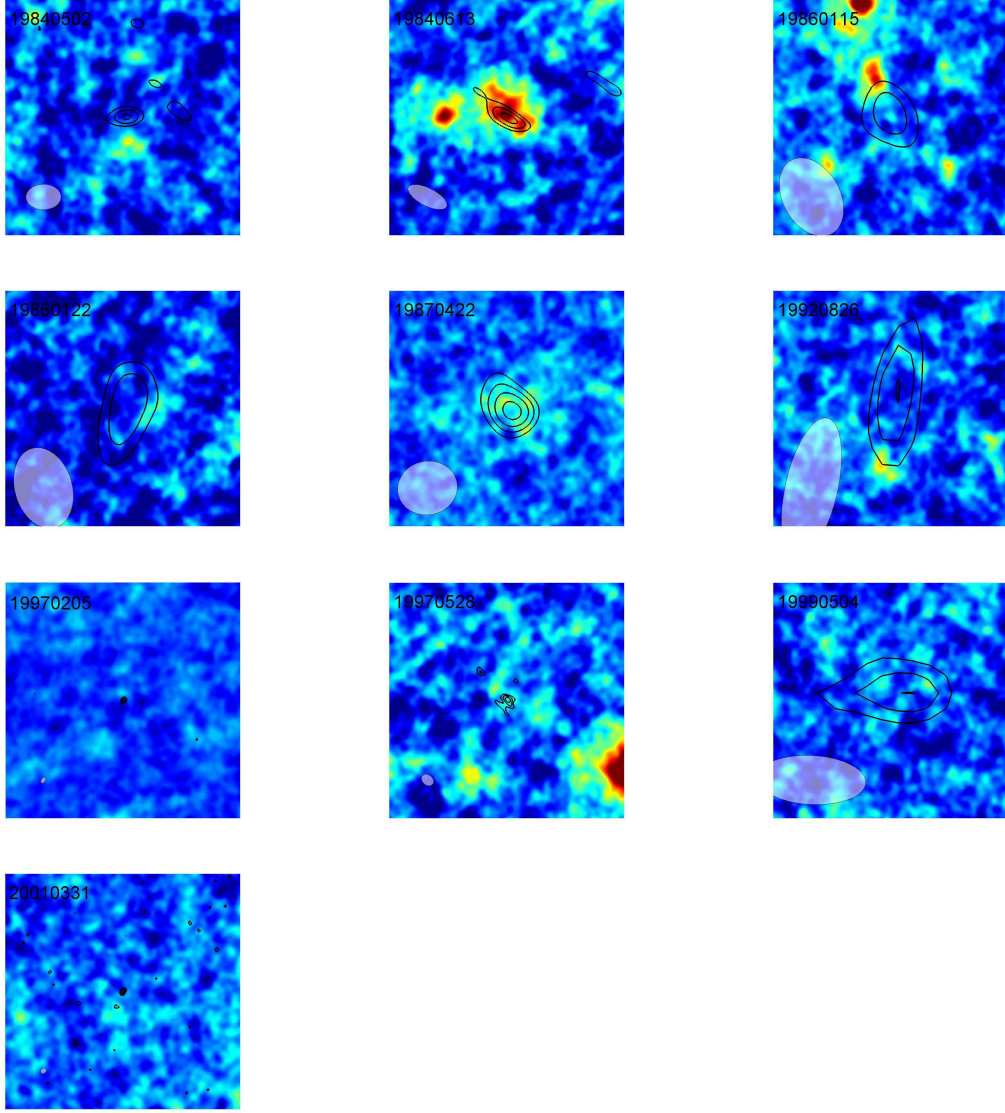
Fig. 5.— Contour plots of transients overlaid on color images from the deep radio image. Each image is 1′ in scale. Contours are 3, 4, 5, 6, and 7 times the image rms. The synthesized beam for each image is displayed in blue in the lower left-hand corner. The color scale of the deep radio image has a range of 0 to 100 μJy.
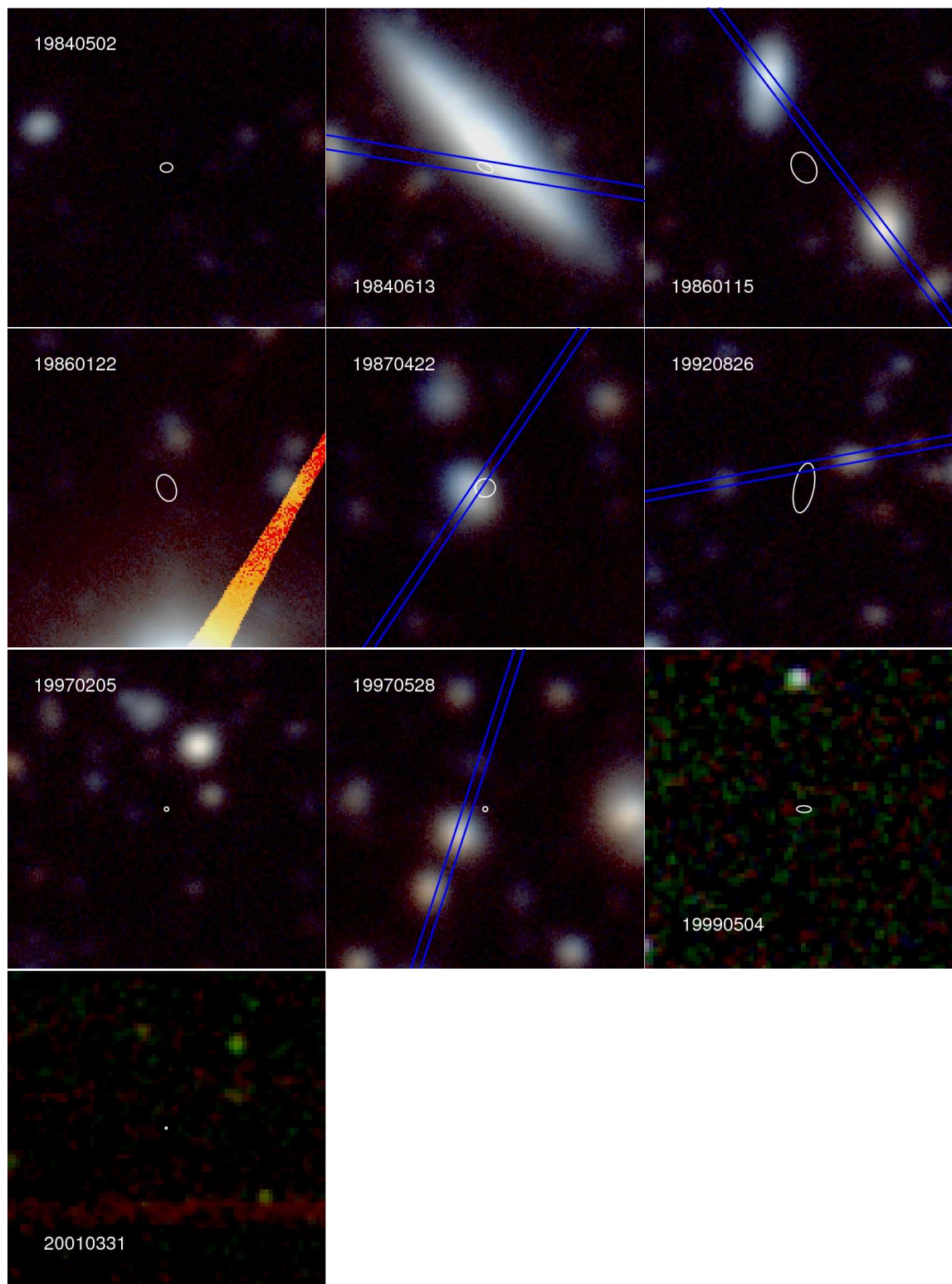
19840502

19840613

19860115

19860122

19870422

19920826

19970205

19970528

19990504

20010331

Fig. 6.— Optical and infrared images at the positions of transient sources. The white circle indicates the uncertainty in the position of the RT. Images are from Keck except for RTs 19990504 and 20010331, which are from PAIRITEL. The color composite for the Keck images was made by using the g-band image for the blue channel, R band for the red channel, and the geometric mean of the two images for the green channel. Keck images are 38″ on a side. The PAIRITEL image is in the K band and is 73″ on a side. The orientation and location of the spectroscopic slit is indicated with blue bars. North is up and east is to the left. The bright streak in the image of RT 19860122 is a diffraction spike from a nearby bright star.
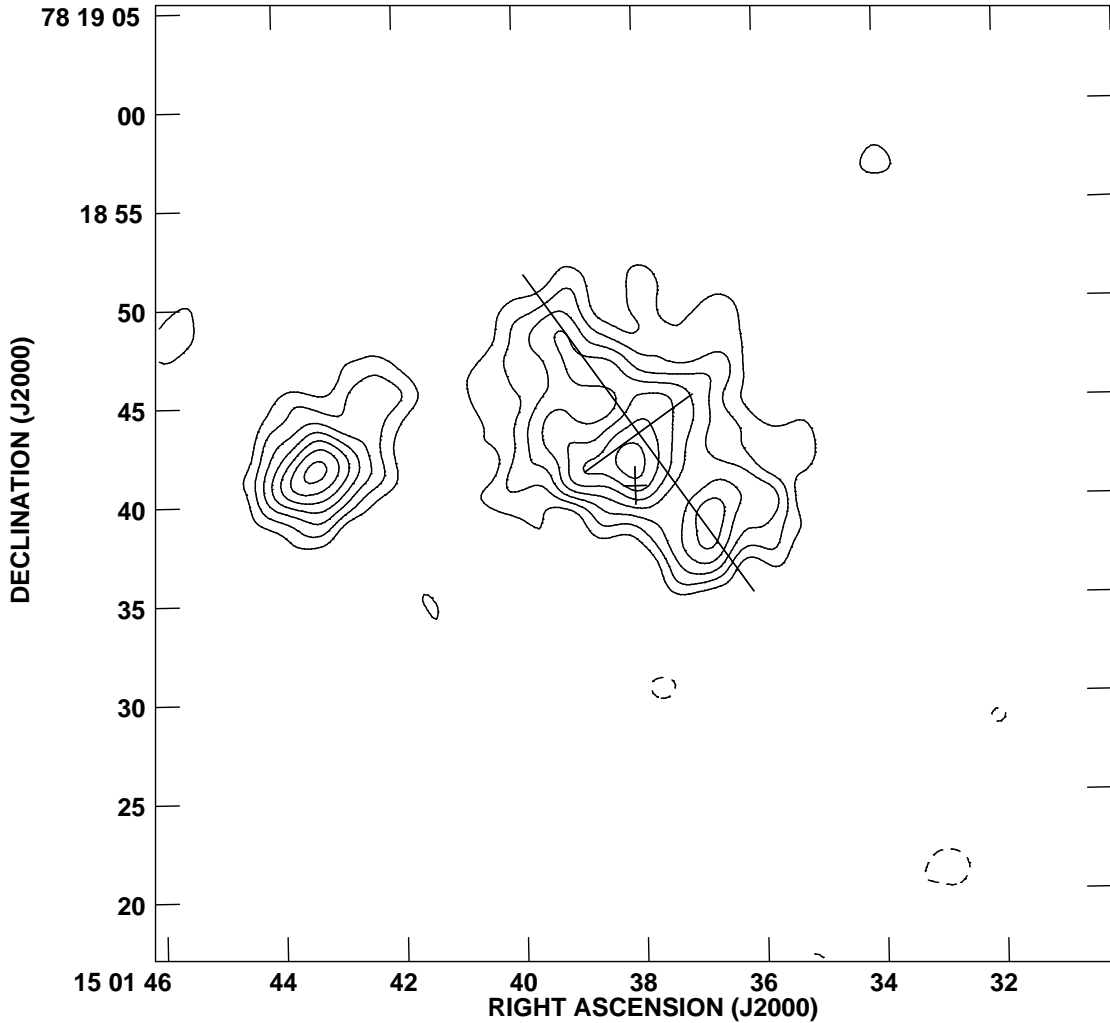

Fig. 7.— Deep image of the region centered on the transient 19840613. The small cross marks the position and 3σ uncertainty in its position. The position is clearly offset from the centroid of the radio emission and from the centroid of the optical emission, marked with

the large cross. The extent of the large cross delineates the major and minor axes of the galaxy as measured in 2MASS. Contours are 3, 4, 5, 6, 7, 8, 9, and 10 times the image rms of 2.6 μJy.

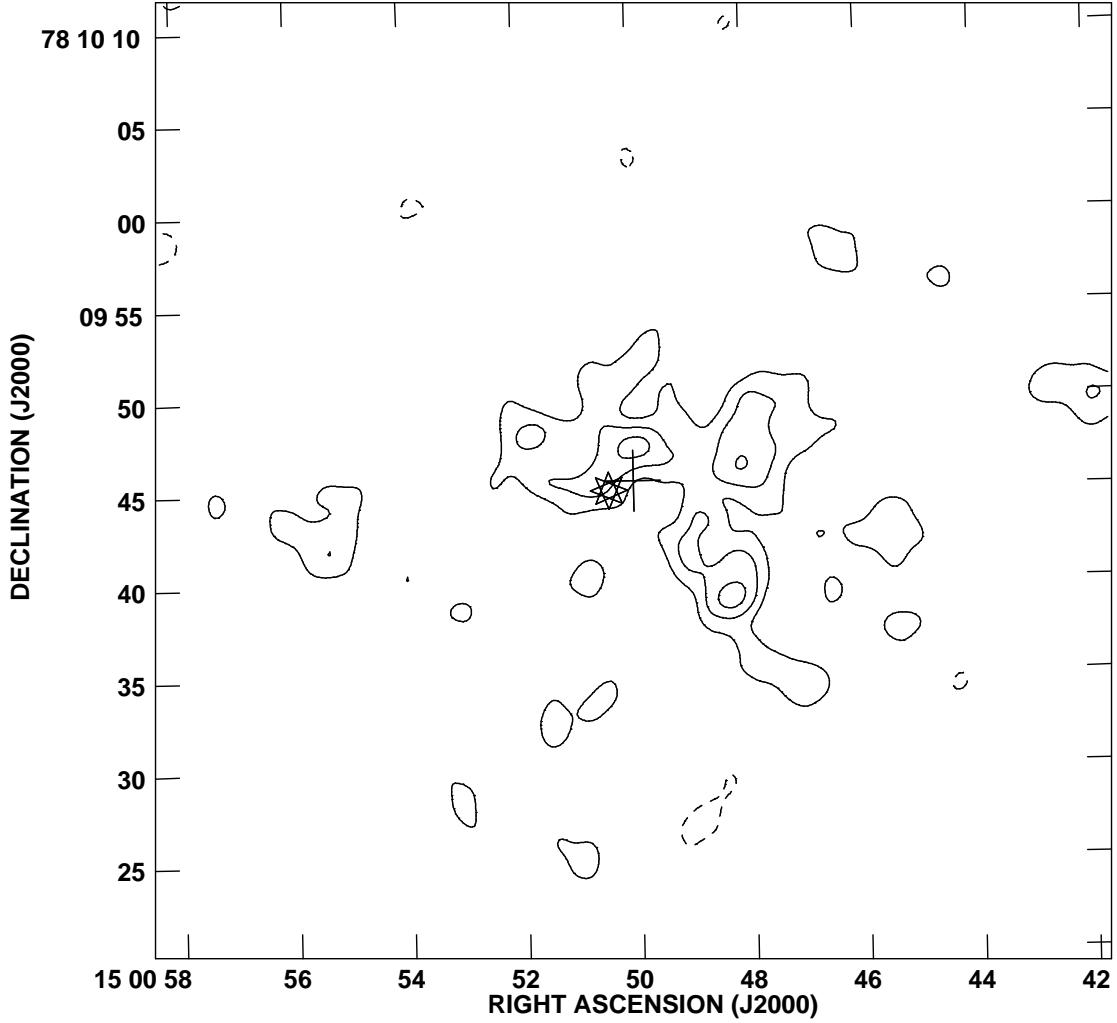Fig. 8.— Deep image of the region centered on the transient 19870422. We mark the position and 3σ uncertainty of the RT (plus sign) and the position of the optical centroid (star). The RT position is offset from any peak of the radio emission but is consistent with the peak of the optical emission. Contours are -2, 2, 3, and 4 times the image rms of 14 μJy at the location of the transient.
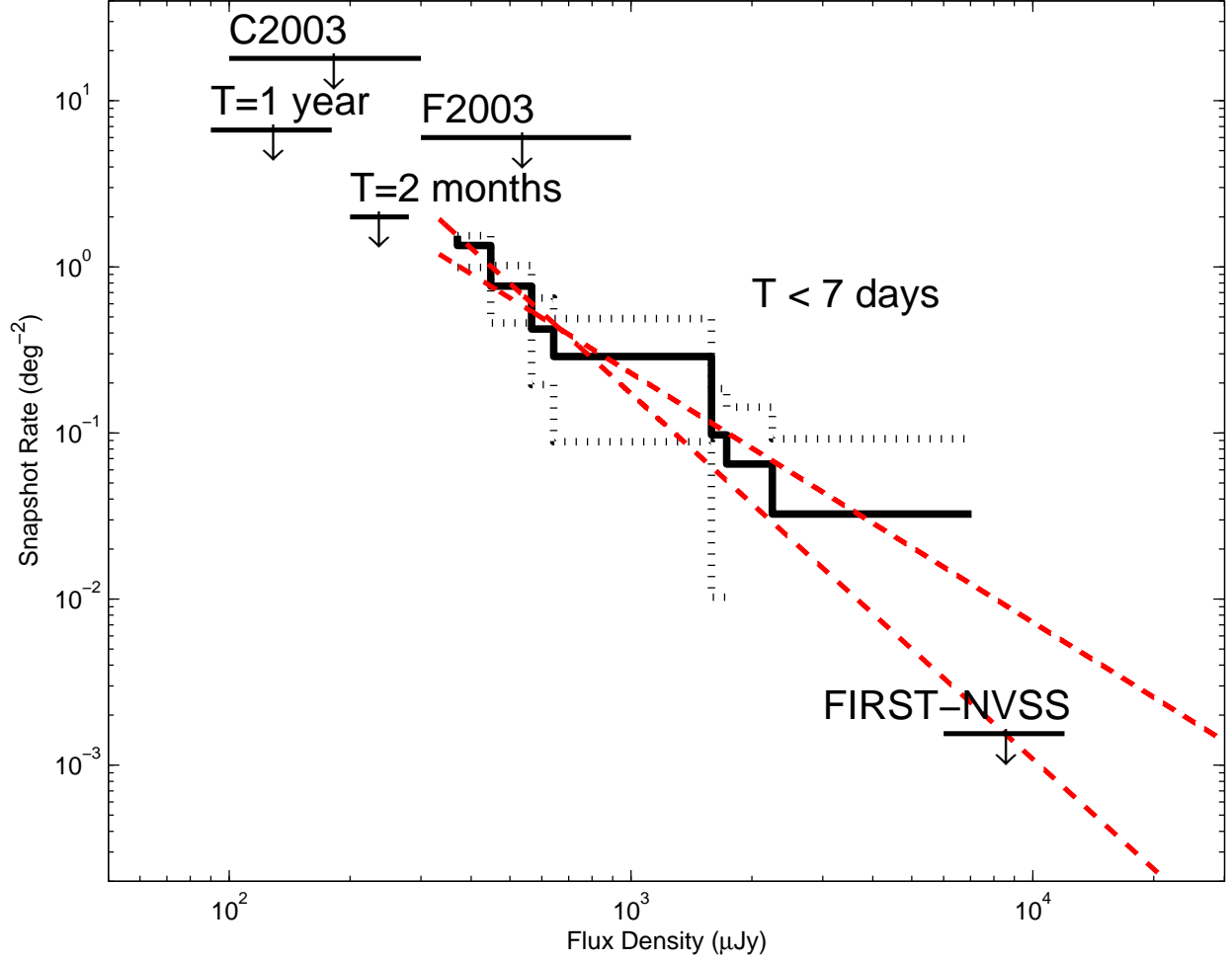
Fig. 9.— The cumulative two-epoch source density for radio transients as a function of flux density. The solid black line shows the rate while the dotted lines show the 2σ upper and lower bounds. The red dashed lines show $S^{-1.5}$ and $S^{-2.2}$ curves. Both are reasonable fits to these data, while the latter shows greater consistency with lower-frequency results. The arrows show 2σ upper limits for transients from this survey with a 1-year timescale, two-month timescale, and for transients from the comparison of the 1.4 GHz NVSS and FIRST surveys (Gal-Yam et al. 2006), from the Carilli et al. (2003) survey (labeled C2003), and from the Frail et al. (2003) survey (labeled F2003). See the main text for details of these surveys.

Table 7.   Effective Area Searched for a Comparable Two-Epoch Survey for $T_{\mathrm{char}} = 1$ year

Flux Density (μJy)	5 GHz Number of Epochs	Area (deg^2)	8.4 GHz Number of Epochs	Area (deg^2)	Total Number of Epochs	Area (deg^2)
50	5	0.02	10	0.02	15	0.04
70	13	0.09	14	0.05	15	0.10
100	17	0.24	15	0.08	20	0.26
140	17	0.38	15	0.14	20	0.42
200	17	0.53	16	0.18	21	0.57
280	17	0.67	16	0.23	21	0.73
400	17	0.82	16	0.27	21	0.89
560	17	0.96	16	0.32	21	1.14
800	17	1.09	16	0.35	21	1.19
1120	17	1.15	16	0.36	21	1.24
1600	17	1.16	16	0.36	21	1.25